

Ground-level gaseous pollutants (NO₂, SO₂, and CO) in China: daily seamless mapping and spatiotemporal variations

Jing Wei^{1*}, Zhanqing Li^{1*}, Jun Wang², Can Li¹, Pawan Gupta^{3,4}, Maureen Cribb¹

1. Department of Atmospheric and Oceanic Science, Earth System Science Interdisciplinary
Center, University of Maryland, College Park, MD, USA

2. Department of Chemical and Biochemical Engineering, Iowa Technology Institute, Center for
Global and Regional Environmental Research, University of Iowa, USA

3. STI, Universities Space Research Association (USRA), Huntsville, AL, USA

4. NASA Marshall Space Flight Center, Huntsville, AL, USA

* Correspondence:

Zhanqing Li (zhanqing@umd.edu) and Jing Wei (weijing_rs@163.com; weijing@umd.edu)

Abstract

Gaseous pollutants at the ground level seriously threaten the urban air quality environment and public health. There are few estimates of gaseous pollutants that are spatially and temporally resolved and continuous across China. This study takes advantage of big data and artificial intelligence technologies to generate seamless daily maps of three major ambient pollutant gases, i.e., NO₂, SO₂, and CO, across China from 2013 to 2020 at a uniform spatial resolution of 10 km. Cross-validation between our estimates and ground observations illustrated a high data quality on a daily basis for surface NO₂, SO₂, and CO concentrations, with mean coefficients of determination (root-mean-square errors) of 0.84 (7.99 µg/m³), 0.84 (10.7 µg/m³), and 0.80 (0.29 mg/m³), respectively. We found that the COVID-19 lockdown had sustained impacts on gaseous pollutants, where surface CO recovered to its normal level in China on around the 34th day after the Lunar New Year, while surface SO₂ and NO₂ rebounded more than twice slower due to more CO emissions from increased residents' indoor cooking and atmospheric oxidation capacity. Surface NO₂, SO₂, and CO reached their peak annual concentrations of 21.3 ± 8.8 µg/m³, 23.1 ± 13.3 µg/m³, and 1.01 ± 0.29 mg/m³ in 2013, then continuously declined over time by 12%, 55%, and 17%, respectively, until 2020. The declining rates were more prominent from 2013 to 2017 due to the sharper reductions in anthropogenic emissions but have slowed down in recent years. Nevertheless, people still suffer from high-frequency risk exposure to surface NO₂ in eastern China, while surface SO₂ and CO have almost reached the recommended air quality guidelines level since 2018, benefiting from the implemented stricter “ultra-low” emission standards. This reconstructed dataset of surface gaseous pollutants will benefit future (especially short-term) air pollution and environmental health-related studies.

1. Introduction

Air pollution has been a major environmental concern, affecting human health, weather, and climate (Anenberg et al., 2022; Kan et al., 2012; Li et al., 2017a; Murray et al., 2020; Orellano et al., 2020), thus drawing worldwide attention. The sources of air pollution are complex. They include natural sources such as wildfires and anthropogenic emissions, including pollutants discharged from industrial production [e.g., smoke/dust, sulfur oxides, nitrogen oxides (NO_x), and volatile organic compounds (VOCs)], hazardous substances released from burning coal during heating seasons [e.g., dust, sulfur dioxide (SO₂), and carbon monoxide (CO)], and waste gases (e.g., CO, SO₂, and NO_x) generated by transportation, especially in big cities.

Among various air pollutants, the following have been most widely recognized: particulate matter with diameters smaller than 2.5 μm and 10 μm (PM_{2.5} and PM₁₀) and gaseous pollutants [e.g., ozone (O₃), nitrogen dioxide (NO₂), SO₂, and CO, among others]. Many countries have built ground-based networks to monitor a variety of conventional pollutants in real time. China has experienced serious ambient air pollution for a long time, prompting the establishment of a large-scale air quality monitoring network (MEE, 2018a). Over the years, much effort has been made to model different species of air pollutants. Many studies focused on particulate matter in China have been carried out (Gao et al., 2022; Li et al., 2017b; Li et al., 2022b; Ma et al., 2022; Yang et al., 2022; Zhang et al., 2018). The global COVID-19 pandemic has motivated many attempts to estimate surface NO₂ concentrations from satellite-retrieved tropospheric NO₂ products (Tian et al., 2020; WHO, 2020), e.g., from the Ozone Monitoring Instrument (OMI) onboard the NASA Aura spacecraft and the TROPOspheric Monitoring Instrument (TROPOMI) onboard the Copernicus Sentinel-5 Precursor satellite, adopting different statistical regression (Chi et al., 2021; Qin et al., 2017; Zhang et al., 2018) and artificial intelligence (Chen et al., 2019; Chi et al., 2022; Dou et al., 2021; Liu, 2021; Wang et al., 2021; Zhan et al., 2018) models. By comparison, surface SO₂ and CO in China are less studied, limited by weaker signals and a lack of good-quality satellite tropospheric products (Han et al., 2022b; Li et al., 2020; Liu et al., 2019; Wang et al., 2021). Such studies still face more challenges, e.g., satellite data gaps and missing values that seriously limit their application and the neglect of spatiotemporal differences in air pollution in the modeling process. In

addition, most previous studies mainly focused on studying a single or a few species during relatively short observational periods.

In view of the above problems, the purpose of this paper is to reconstruct daily concentrations of three ambient gaseous pollutants (i.e., NO₂, SO₂, and CO) in China. To this end, relying on the dense national ground-based observation network and big data, including satellite remote sensing products, meteorological reanalysis, chemical model simulations, and emission inventories, we are capable of mapping three pollutant gases seamlessly (100% spatial coverage) on a daily basis at a uniform spatial resolution of 10 km since 2013 in China. Estimates were made using an extended and powerful machine-learning model incorporating spatiotemporal information, i.e., space-time extra-trees. Natural and anthropogenic effects on air pollution, including their physical mechanisms and chemical reactions, were accounted for in the modeling. Using this dataset, spatiotemporal variations of the gaseous pollutants, the impacts of environmental protection policies and the COVID-19 epidemic, and population risk exposure to gaseous pollution are investigated.

To date, we have combined the advantages of artificial intelligence and big data to construct a virtually complete set of major air quality parameters concerning both particulate and gaseous pollutants over a long period of time across China, including PM₁ (1 km, 2000–Present) (Wei et al., 2019), PM_{2.5} (1 km, 2000–Present) (Wei et al., 2020; Wei et al., 2021a), PM₁₀ (1 km, 2000–Present) (Wei et al., 2021b), O₃ (10 km, 1979–Present) (Wei et al., 2022a; He et al., 2022b), and NO₂ (1 km, 2019–Present) (Wei et al., 2022b), serving environmental, public health, economy, and other related research. This study is the continuation of our previous studies, which adds two new species of SO₂ and CO for the first time and also dates the data records of NO₂ back to 2013. Instead of devoting itself to a single pollutant, this study deals with all gaseous pollutants of compatible quality over the same period with the same spatial coverage and resolution. In particular, considering that there are few public datasets of these three gaseous pollutants with such spatiotemporal coverages focusing on the whole of China, this is highly valuable for the sake of studying their variations, relative proportions, and attribution of emission sources, as well as their diverse and joint effects of different pollutant species on public health.

2. Materials and methods

2.1 Big data

2.1.1 Ground-based measurements

Hourly measurements of ground-level NO₂, SO₂, and CO concentrations from ~1600 reference-grade ground-based monitoring stations (Figure 1) collected from the China National Environmental Monitoring Centre (CNEMC) network were employed in the study. This network includes urban assessing stations, regional assessing stations, background stations, source impact stations, and traffic stations, set up in a reasonable overall layout that covers industrial (~14%), urban (~31%), suburban (~39%), and rural (~16%) areas to improve the spatial representations, continuity, and comparability of observations (HJ 664-2013) (MEE, 2013a). NO₂ is measured by chemiluminescence and differential optical absorption spectroscopy (DOAS), and SO₂ uses ultraviolet fluorescence and DOAS, while CO adopts non-dispersive infrared spectroscopy and gas filter correlation infrared spectroscopy. These measurements have been fully validated and have the same average error of indication of $\pm 2\%$ F.S. for the three gaseous pollutants considered here, with additional quality-control checks such as zero and span noise and zero and span drift (HJ 193-2013 and HJ 654-2013) (MEE, 2013b, 2013c). They have also been used as ground truth in almost all air pollutant modelling studies in China (Ma et al., 2022; Zhang et al., 2022a). All stations use the same technique to measure each gas routinely and continuously 24 hours a day at about the sea level without time series gaps. However, the reference state (i.e., observational conditions like temperature and pressure) changed from the standard condition (i.e., 273 K and 1013 hPa) to the room condition (i.e., 298 K and 1013 hPa) on 31 August 2018 (MEE, 2018a). We thus first converted observations of the three gaseous pollutants after this date to the uniform standard condition for consistency. Here, daily values for each air pollutant were averaged from at least 30% of valid hourly measurements at each station in each year from 2013 to 2020.

[Please insert Figure 1 here]

2.1.2 Main predictors

A new daily tropospheric NO₂ dataset at a horizontal resolution of $0.25^\circ \times 0.25^\circ$ in China was employed, created using a developed framework integrating OMI/Aura Quality Assurance for Essential Climate Variables (QA4ECV) and Global Ozone Monitoring Experiment-2B (GOME-2B)

offline tropospheric NO₂ retrievals passing quality controls (i.e., cloud fraction < 0.3, surface albedo < 0.3, and solar zenith angle < 85°) (He et al., 2020). The reconstructed tropospheric NO₂ agreed well ($R = 0.75\text{--}0.85$) with Multi-AXis Differential Optical Absorption Spectroscopy (MAX-DOAS) measurements. Through this data fusion, the daily spatial coverage of satellite tropospheric NO₂ was significantly improved in China (average = 87%). Areas with a small number of missing values were imputed via a nonparametric machine-learning model by regressing the conversion relationship with Copernicus Atmosphere Monitoring Service (CAMS) tropospheric NO₂ assimilations ($0.75^\circ \times 0.75^\circ$), making sure that the interpolation was consistent with the OMI/Aura overpass time (Inness et al., 2019; Wang et al., 2020b). The gap-filled tropospheric NO₂ was reliable compared with measurements ($R = 0.94\text{--}0.98$) (Wei et al., 2022b). The above two-step gap-filling procedures allowed us to generate a daily seamless tropospheric NO₂ dataset that removes the effects of clouds from satellite observations.

Here, the reconstructed daily seamless tropospheric NO₂, together with CAMS daily ground-level NO₂ assimilations ($0.75^\circ \times 0.75^\circ$) averaged from all 3-hourly data in a day and monthly NO_x anthropogenic emissions ($0.1^\circ \times 0.1^\circ$) (Inness et al., 2019), were used as the main predictors for estimating surface NO₂. Limited by the quality of direct satellite observations, daily model-simulated SO₂ and CO surface mass concentrations, averaged from all available data in a day provided by one-hourly Modern-Era Retrospective Analysis for Research and Applications, version 2 (MERRA-2, $0.625^\circ \times 0.5^\circ$), 3-hourly CAMS ($0.75^\circ \times 0.75^\circ$), and 3-hourly Goddard Earth Observing System Forward-Processing ($0.3125^\circ \times 0.25^\circ$) global reanalyses were used as main predictors to retrieve surface SO₂ and CO, together with CAMS monthly SO₂ and CO anthropogenic emissions.

145

146 **2.1.3 Auxiliary factors**

Meteorological factors have important diverse effects on air pollutants (He et al., 2017; Li et al., 2019), e.g., the boundary-layer height reflects their vertical distribution and variations (Li et al., 2017a; Seo et al., 2017); temperature, humidity, and pressure can affect their photochemical reactions (Li et al., 2019; Xu et al., 2011; Zhang et al., 2019a); and rainfall and wind can also influence their removal, accumulation, and transport (Dickerson et al., 2007; Li et al., 2019). Eight

152 daily meteorological variables, provided by the ERA5-Land ($0.1^\circ \times 0.1^\circ$) (Muñoz-Sabater et al.,
153 2021) and ERA5 global reanalysis ($0.25^\circ \times 0.25^\circ$) (Hersbach et al., 2020), were calculated (i.e.,
154 accumulated for precipitation and evaporation while averaged for the others) from all hourly data in
155 a day, used as auxiliary variables to improve the modelling of gaseous pollutants. Other auxiliary
156 remote-sensing data used to describe land-use cover/change [i.e., Moderate Resolution Imaging
157 Spectroradiometer (MODIS) normalized difference vegetation index (NDVI), $0.05^\circ \times 0.05^\circ$] and
158 population distribution density (i.e., LandScanTM, 1 km) were employed as inputs to the machine-
159 learning model because they are highly related to the type of pollutant emission and amounts of
160 anthropogenic emissions, as well as the surface terrain [i.e., Shuttle Radar Topography Mission
161 (SRTM) digital elevation model (DEM), 90m], which can affect the transmission of air pollutants.
162 Table S1 provides detailed information about all the data used in this study. All variables were
163 aggregated or resampled into a $0.1^\circ \times 0.1^\circ$ resolution for consistency.

164

165 **2.2 Pollutant gas modelling**

166 Here, the developed Space-Time Extra-Tree (STET) model, integrating spatiotemporal
167 autocorrelations of and differences in air pollutants to the Extremely Randomized Trees (ERT) (Wei
168 et al., 2022a), was extended to estimate surface gaseous pollutants, i.e., NO₂, SO₂, and CO. ERT is
169 an ensemble machine-learning model based on the decision tree, capable of solving the
170 nonparametric multivariable nonlinear regression problem. Ensemble learning can avoid the lack of
171 learning ability of a single learner, greatly improving accuracy. The introduced randomness
172 enhances the model's anti-noise ability and minimizes the sensitivity to outliers and
173 multicollinearity issues. It can handle high latitude, discrete or continuous data without data
174 normalization and is easy to implement and parallel. However, several limitations exist, e.g., it is
175 difficult to make predictions beyond the range of training data, and there will be an over-fitting
176 issue on some regression problems with high noise. The training efficiency diminishes with
177 increasing memory occupation when the number of decision trees is large (Geurts et al., 2006).
178 Compared with traditional tree-based models (e.g., random forest), ERT has a stronger randomness
179 which randomly selects a feature subset at each node split and randomly obtains the optimal branch
180 attributes and thresholds. This helps to create more independent decision trees, further reducing

model variance and improving training accuracy (Geurts et al., 2006). The STET model has been successfully applied in estimating high-quality surface O_3 in our previous study (Wei et al., 2022a). It is thus extended here to regress the nonlinear conversion relationships between ground-based measurements and the main predictors and auxiliary factors for other species of gaseous pollutants. For surface NO_2 , the STET model was applied to the main variables of the satellite tropospheric NO_2 column, modelled surface NO_2 mass, and NO_x emissions, together with ancillary variables of the previously mentioned meteorological, surface, and population variables (Equation 1). For surface SO_2 (Equation 2) and CO (Equation 3), modelled surface SO_2 and CO concentrations and SO_2 and CO emissions were used as main predictors along with the same auxiliary variables as NO_2 to construct the STET models separately.

$$NO_{2(ijt)} \sim f_{STET}(SNO_{2(ijt)}, MNO_{2(ijt)}, ENO_{x_{ijm}}, Meteorology_{ijt}, NDVI_{ijm}, DEM_{ijy}, POP_{ijy}, P_s, P_t), \quad (1)$$

$$SO_{2(ijt)} \sim f_{STET}(MSO_{2(ijt)}, ESO_{2(ijm)}, Meteorology_{ijt}, NDVI_{ijm}, DEM_{ijy}, POP_{ijy}, P_s, P_t), \quad (2)$$

$$CO_{ijt} \sim f_{STET}(MCO_{ijt}, ECO_{ijm}, Meteorology_{ijt}, NDVI_{ijm}, DEM_{ijy}, POP_{ijy}, P_s, P_t), \quad (3)$$

where $NO_{2(ijt)}$, $SO_{2(ijt)}$, and CO_{ijt} indicate daily ground-based NO_2 , SO_2 , and CO measurements at one grid (i, j) on the t th day of a year; $SNO_{2(ijt)}$ indicates the daily satellite tropospheric NO_2 column at one grid (i, j) on the t th day of a year; $MNO_{2(ijt)}$, $MSO_{2(ijt)}$, and MCO_{ijt} indicate daily model-simulated surface NO_2 , SO_2 , and CO concentrations at one grid (i, j) on the t th day of a year; $ENO_{x_{ijm}}$, $ESO_{2(ijm)}$, and ECO_{ijm} indicate monthly anthropogenic NO_x , SO_2 , and CO emissions at one grid (i, j) in the m th month of a year; $Meteorology_{ijt}$ represents each meteorological variable at one grid (i, j) on the t th day of a year; DEM_{ijy} and POP_{ijy} indicate the elevation and population at one grid (i, j) of a year; and P_s and P_t indicate the space and time terms (Wei et al., 2022a).

3. Results and discussion

3.1 Seamless mapping of surface gaseous pollutants

Using the constructed STET model, we generated daily 10 km resolution datasets with complete coverage (spatial coverage = 100%) for three ground-level gaseous pollutants from 2013 to 2020 in China, called ChinaHigh NO_2 , ChinaHigh SO_2 , and ChinaHighCO. Monthly and annual maps were

210 generated by directly averaging daily data at each grid. They belong to a series of public long-term,
211 full-coverage, high-resolution, and high-quality datasets of a variety of ground-level air pollutants
212 for China [ChinaHighAirPollutants (CHAP)] developed by our team. Figure 2 shows spatial
213 distributions of the three pollutant gases across China on a typical day (1 January 2018). The spatial
214 patterns of these gaseous pollutants were consistent with those observed on the ground, especially
215 in highly polluted areas, e.g., severe surface NO₂ pollution in the North China Plain (NCP) and high
216 surface SO₂ emissions in Shanxi Province. The unique advantage of our dataset is that it can
217 provide valuable gaseous pollutant information on a daily basis at locations in China where ground
218 measurements are not available. This addresses the major issues of scanning gaps and numerous
219 missing values in satellite remote sensing retrievals at cloudy locations, e.g., the average spatial
220 coverage of the official OMI/Aura daily tropospheric NO₂ product is only 42% over the whole of
221 China during the period 2013–2020 (Figure S1). Our dataset provides spatially complete coverage,
222 significantly increasing daily satellite observations by 58%. In addition, reanalysis data do not
223 simulate surface masses of gaseous pollutants well, underestimating them compared to our results
224 and ground-based observations in China (Figure S2). This is especially so for SO₂, where high-
225 pollution hot spots are easily misidentified. Validation illustrates that our regressed results for
226 surface NO₂, SO₂, and CO agree better with ground measurements than modelled results (slopes are
227 close to 1, and correlations > 0.93), 1.9–6.4 times stronger in slope, 1.3–3.5 times higher in
228 correlation, but 5.9–7.7 times smaller in differences (Figure S3). This shows that our model can take
229 advantage of big data to significantly correct and reconstruct gaseous simulation results via data
230 mining using machine learning.

231 *[Please insert Figure 2 here]*

232 Figure 3 shows annual and seasonal maps for each gas pollutant during the period 2013–2020
233 across China. Multi-year mean surface NO₂, SO₂, and CO concentrations were $20.3 \pm 4.7 \mu\text{g}/\text{m}^3$,
234 $16.2 \pm 7.7 \mu\text{g}/\text{m}^3$, and $0.86 \pm 0.22 \text{ mg}/\text{m}^3$, respectively. Pollutant gases varied significantly in space
235 across China, where high surface NO₂ levels were mainly distributed in typical urban
236 agglomerations, e.g., the Beijing-Tianjin-Hebei (BTH) region, the Yangtze River and Pearl River
237 Deltas (YRD and PRD), and scattered large cities with intensive human activities and highly

238 developed transportation systems (e.g., Urumqi, Chengdu, Xi'an, and Wuhan, among others). High
239 surface SO₂ concentrations were mainly observed in northern China (e.g., Shanxi, Hebei, and
240 Shandong Provinces), associated with combustion emissions from anthropogenic sources, and the
241 Yunnan Guizhou Plateau in southwest China, likely associated with emissions from volcanic
242 eruptions. By contrast, except in some areas in central China (e.g., Shanxi and Hebei), surface CO
243 concentrations were overall low.

244 Significant differences in spatial patterns were seen at the seasonal level. Surface NO₂, SO₂, and CO
245 in summer (average = $15.9 \pm 4.7 \mu\text{g}/\text{m}^3$, $22.9 \pm 13.4 \mu\text{g}/\text{m}^3$, and $1.1 \pm 0.3 \text{ mg}/\text{m}^3$, respectively) were
246 the lowest, thanks to favorable meteorological conditions, e.g., abundant precipitation and high air
247 humidity conducive to flushing and scavenging of different air pollutants (Yoo et al., 2014). Strong
248 sunlight and high temperature also accelerate the photochemical reactions of NO₂ loss (Shah et al.,
249 2020). Pollution levels were highest in winter, with average values increasing by ~1.5–1.9 times
250 those in summer. This difference was much larger in central and eastern China, e.g., 2.3–3.4 times
251 higher in the BTH due to large amounts of direct NO_x, SO₂, and CO emissions from burning coal
252 for heating in winter in northern China. The spatial patterns of the three gaseous pollutants were
253 similar in spring and autumn.

254 *[Please insert Figure 3 here]*

255 **3.2 Changes in gaseous pollution and exposure risk**

256 **3.2.1 Short-term epidemic effects on air quality**

257 Many studies have focused on the effects of the COVID-19 epidemic on air quality (WHO, 2020).
258 Most of them were done using ground-based observations (Huang et al., 2020; Su et al., 2020),
259 tropospheric gas columns (Field et al., 2021; Levelt et al., 2022), or retrieved surface masses
260 (Cooper et al., 2022; Ling and Li, 2021). The resulting conclusions could be affected by insufficient
261 spatial representation due to the uneven distribution of ground monitors or a large number of
262 missing values in space due to the influence of clouds. The unique advantage of our seamless day-
263 to-day gaseous pollutant dataset can make up for these shortcomings, allowing us to assess the
264 changes more accurately and quantitatively in gaseous pollutants during the epidemic.

265 We first compared the spatial differences in monthly relative differences from February to April

266 between 2020 and 2019 in China (Figure 4). In February, surface NO₂ sharply reduced in China,
267 especially in key urban agglomerations and megacities, showing relative changes of greater than
268 50%. A significant decrease in surface SO₂ (> 40%) was observed in northern areas where heavy
269 industry is the mainstay in China (e.g., Tianjin, Hebei, and Shandong), while little change was seen
270 in southern China. Surface CO also showed drastic decreases, but the amplitude was smaller than
271 the other two gaseous pollutants. These were attributed to extensive plant closures and traffic
272 controls due to the lockdown, which started at the end of January 2020, significantly reducing
273 anthropogenic NO_x, SO₂, and CO emissions (Ding et al., 2020; Yang et al., 2022; Zheng et al.,
274 2021). In March, surface NO₂ was still generally lower than the historical level in most eastern
275 areas, especially in areas where the epidemic was severe, i.e., Wuhan, Hubei Province, and its
276 surrounding areas. The decrease in surface SO₂ largely slowed by more than two times in the NCP
277 and central China, while surface CO almost returned to normal levels in most areas in China. In
278 April, surface NO₂ and SO₂ were comparable to historical concentrations (within $\pm 10\%$), even
279 increasing in some areas of southern and northeastern areas due to rebounding anthropogenic
280 emissions (Ding et al., 2020), especially in Hubei Province, indicating that their surface levels were
281 almost recovered.

282 *[Please insert Figure 4 here]*

283 Most previous studies have focused mainly on changes during the lockdown, with little attention
284 paid to the recovery. We thus compared the time series of daily population-weighted concentrations
285 of the three gaseous pollutants after the Lunar New Year between 2020 and 2019 in China (Figure
286 5). After the beginning of New Year's Eve, surface gaseous pollutants showed a significant decrease
287 in both the normal and epidemic years due to the closure of factories, with decreasing
288 anthropogenic emissions during the Spring Festival holiday. However, gaseous pollutants in the
289 normal year rose rapidly after they fell to their lowest levels due to the return to work after the
290 holidays. By contrast, their levels continued to decrease in 2020 and were lower than historical
291 levels due to the sustained impacts of the strict lockdowns. They hit bottom in the 4th week after the
292 Lunar New Year, then began to increase gradually. Surface NO₂ and SO₂ recovered in the middle of
293 the 11th week (around the 72nd and 75th days) after the Lunar New Year (i.e., 2020 and 2019

concentrations intersected and then alternately changed). However, surface CO levels recovered at the end of the 5th week (around the 34th day), more than twice faster than NO₂ and SO₂ levels. This is attributed to more CO emissions from increased residents' indoor cooking (Zheng et al., 2018), increased atmospheric oxidation capacity (Huang et al., 2020; Wei et al., 2022a), and a potentially higher sensitivity to temperature rises (Lin et al., 2021).

[Please insert Figure 5 here]

3.2.2 Temporal variations and policy implications

Figures S4-S6 show annual mean maps of each gaseous pollutant from 2013 to 2020 in China. Surface NO₂, SO₂, and CO changed greatly, peaking in 2013, with average values of $21.3 \pm 8.8 \mu\text{g}/\text{m}^3$, $23.1 \pm 13.3 \mu\text{g}/\text{m}^3$, and $1.01 \pm 0.29 \text{ mg}/\text{m}^3$, respectively. They reached their lowest levels in 2020, particularly due to the noticeable effects of the COVID-19 epidemic. In general, national ambient NO₂, SO₂, and CO concentrations decreased by approximately 12%, 55%, and 17% from 2013 to 2020, respectively. Large seasonal differences were observed in the amplitude of gaseous pollutant (Figure 6), e.g., surface NO₂ decreased the most in winter, especially in the three urban agglomerations ($\downarrow 24\text{--}31\%$), changing the least in autumn (especially in the YRD). Surface SO₂ showed much larger decreases in all seasons, especially during the cold seasons ($\downarrow 55\text{--}81\%$), due to the implementation of stricter “ultra-low” emission standards (Li et al., 2022a; Zhang et al., 2019b). Surface CO had similar seasonal changes as SO₂ but 1.5–3.3 times smaller in amplitude.

[Please insert Figure 6 here]

To better investigate the spatiotemporal variations of ambient gaseous pollution, we calculated linear trends and significance levels using monthly anomalies by removing seasonal cycles. Most of China showed significant decreasing trends, with average annual rates of $0.23 \mu\text{g}/\text{m}^3$, $2.01 \mu\text{g}/\text{m}^3$, and $0.05 \text{ mg}/\text{m}^3$ for surface NO₂, SO₂, and CO ($p < 0.001$), respectively (Figure 7), especially in three urban agglomerations and large cities (e.g., Wuhan and Chengdu). The largest downward trends mainly occurred in northern and central China, especially in the BTH (Table 3). This is mainly due to the change in fuel for heating from coal to gas widespread across China in winter (Wang et al., 2020a), greatly reducing emissions of precursor gases (Koukouli et al., 2018).

Increasing trends of surface NO₂ were, however, found in Ningxia and Shanxi Provinces in central China due to increased traffic emissions and new coal-burning power plants in underdeveloped areas without strict regulations on NO_x emissions (Li et al., 2022a; Maji and Sarkar, 2020; Van Der A et al., 2017).

We then divided the study period into three periods to investigate the impact of major environmental protection policies on air quality implemented in China (Figure 7). During the Clear Air Action Plan (CAAP, 2013–2017), the rates of decrease for surface NO₂, SO₂, and CO accelerated in most populated areas in China, especially urban areas. This was due to dramatic reductions in main pollutant emissions like SO₂ and NO_x (by 59% and 21%, respectively) through the upgrading of key industries, industrial structure adjustments, and coal-fired boiler remediation (Zhang et al., 2019b). In addition, the majority of gaseous pollutants had dropped continuously during the Blue Sky Defense War (BSDW, 2018–2020), benefiting from continuous reductions in total air pollutant emissions and the impacts of COVID-19 (Jiang et al., 2021; Zheng et al., 2021). However, areas with trends passing the significance level sharply shrank, especially for surface SO₂. During the 13th Five-Year-Plan (FYP, 2016–2020), the decreasing trends of the three gaseous pollutants across China slowed down compared to those during CAAP. Large decreases in surface NO₂ were mainly found in the BTH region and Henan Province, while slightly increasing trends occurred in southern China. Surface SO₂ significantly decreased in most areas, where a greater downward trend was observed in Shanxi Province, mainly due to the reduction in coal consumption thanks to a strengthened clean-heating policy (Lee et al., 2021). Surface CO also continuously decreased, more rapidly in central China but less rapidly elsewhere. The continuous decline in gaseous pollutants is due to the binding reductions in total emissions of major pollutants like NO_x (↓71%) and SO₂ (↓48%) in China (Wan et al., 2022; Wu et al., 2022c).

[Please insert Figure 7 here]

3.2.3 Population-risk exposure to gaseous pollution

With the daily seamless datasets, we can evaluate the spatial and temporal variations of short-term population-risk exposure to the three gaseous pollutants by calculating the number of days in a given year exceeding the new recommended short-term minimum interim target (IT1) and desired

349 air quality guidelines (AQG) level defined by the WHO in 2021 (WHO, 2021). The area exceeding
350 the recommended levels (i.e., daily $\text{NO}_2 > 120 \mu\text{g}/\text{m}^3$, $\text{SO}_2 > 125 \mu\text{g}/\text{m}^3$, and $\text{CO} > 7 \text{ mg}/\text{m}^3$) was
351 generally small in eastern China (Figure S7). High NO_2 -exposure risks were mainly found in
352 Beijing and Hebei Province and a handful of big cities (e.g., Jinan, Wuhan, Shanghai, and
353 Guangzhou), while high SO_2 -exposure risks were mainly observed in Hebei, Shandong, and
354 Shaanxi Provinces. The risk of high CO pollution was small, only found in some scattered areas in
355 the NCP. In general, both the area and the possibility of occurrence exposure to high pollution has
356 gradually decreased over time, almost disappearing since 2018.

357 By contrast, most areas of eastern China had a surface NO_2 exposure exceeding the AQG level
358 (Figure 8), especially in the north and economically developed areas in the south (proportion >
359 80%). Both the extent and intensity are decreasing over time, but it is still a problem, suggesting
360 that stronger NO_x controls are needed in the future. Most of the main air pollution transmission belt
361 in China (i.e., the “2 + 26” cities, Figure 1) had surface SO_2 levels exceeding the AQG level at the
362 beginning of the study period. Thanks to strict control measures, these polluted areas sharply
363 decreased after 2015, almost disappearing in 2020. Controlling CO was much more successful in
364 China, with less than 10% of the days in the BTH exceeding the acceptable standard in the early
365 part of the study period. Most areas have reached the CO AQG level since 2018.

366 *[Please insert Figure 8 here]*

367 Figure 9 shows the percentage of days with pollution levels exceeding WHO air quality standards in
368 three key regions. BTH was the only region experiencing high NO_2 and SO_2 exposure risks (i.e.,
369 daily mean > IT1), dropping to zero since 2017 and 2016, while YRD and PRD had no high risks of
370 exposure to the three gaseous pollutants (Figure 9a-b). There was also no regional high CO-
371 pollution risk (Figure 9c). However, although declining continuously, regional surface NO_2 levels
372 failed to meet the short-term AQG level in 2020, with 61–73% of the days exceeding the AQG level.
373 More efforts toward mitigating NO_2 levels in these key regions are thus needed. Continual
374 decreases in the number of days above the AQG level were also observed in surface SO_2 , reducing
375 to near zero in 2014, 2016, and 2018 in the PRD, YRD, and BTH, respectively. Less than 3% of the
376 days in the BTH and YRD had surface CO levels exceeding the AQG level. Surface CO levels were

377 always below the AQG level in the PRD.

378 *[Please insert Figure 9 here]*

379 **3.3 Data quality assessment**

380 Here, the widely used out-of-sample 10-fold cross-validation (10-CV) method was adopted to
381 evaluate the overall estimation accuracy of gaseous pollutants (Rodriguez et al., 2010; Wei et al.,
382 2022a). An additional out-of-station 10-CV approach was used to validate the prediction accuracy
383 of gaseous pollutants, performed based on measurements from ground monitoring stations. These
384 measurements were randomly divided into ten subsets, of which data samples from nine subsets
385 were used for model training and the remaining subset for model validation. This was done 10 times,
386 in turn, to ensure that data from all stations were tested. This procedure generates independent
387 training samples and test samples made in different locations, used to indicate the spatial prediction
388 ability of the model in areas where ground-based measurements are unavailable (Wei et al., 2022a;
389 Wu et al., 2021).

390

391 **3.3.1 Estimate and prediction accuracy**

392 Figure 10 shows the CV results of all daily estimates and predictions for ground-level NO₂, SO₂,
393 and CO concentrations from 2013 to 2020 in China (sample size: $N \approx 3.6$ million). Surface NO₂
394 and SO₂ concentrations mainly fell in the range of 200 to 500 $\mu\text{g}/\text{m}^3$. Daily estimates were highly
395 correlated to observations, with the same coefficients of determination ($R^2 = 0.84$) and slopes close
396 to 1 (0.86 and 0.84, respectively). Average root-mean-square error (RMSE) [mean absolute error
397 (MAE)] values of surface NO₂ and SO₂ estimates were 7.99 (5.34) and 10.07 (4.68) $\mu\text{g}/\text{m}^3$, and
398 normalized RMSE (NRMSE) values were 0.25 and 0.51, respectively. Most daily CO observations
399 were less than 10 mg/m^3 , agreeing well with our daily estimates ($R^2 = 0.80$, slope = 0.79), and the
400 average RMSE (MAE) and NRMSE values were 0.29 (0.16) mg/m^3 and 0.3. Compared to
401 estimation accuracies (Figure 10a-c), prediction accuracies slightly decreased, which is acceptable
402 considering the weak signals of trace gases. Daily surface SO₂, NO₂, and CO predictions (Figure
403 10d-f) agree well with ground measurements, with spatial R^2 values of 0.70, 0.68, and 0.61,
404 respectively. Their respective RMSE (MAE) values were 14.28 (8.1) $\mu\text{g}/\text{m}^3$, 11.57 (7.06) $\mu\text{g}/\text{m}^3$,

405 and 0.42 (0.24) mg/m³, and NRMSE values were 0.35, 0.71, and 0.42, respectively, representing the
406 accuracy for areas without ground monitoring stations.

407 *[Please insert Figure 10 here]*

408 The performance of our air pollution modelling was also evaluated on an annual basis, showing that
409 our model works well in estimating and predicting the concentrations of different surface gaseous
410 pollutants in different years (Table 1). The model performance has continuously improved over time,
411 as indicated by increasing correlations and decreasing uncertainties. This is because of the
412 increasing density of ground stations (especially in the suburban areas of cities) and updated quality
413 control of measurements, e.g., improving the sampling flow calibration of monitoring instruments,
414 flow calibration of dynamic calibrators, and revision of precision/accuracy review and data validity
415 judgment (HJ 818-2018) (MEE, 2018b). This has led to an increase in the number of data samples
416 (e.g., from 169 thousand in 2013 to more than 522 thousand in 2020) and improvement in their
417 quality.

418 *[Please insert Table 1 here]*

419 Figure 11 shows the spatial validation of estimated daily pollutant gases across China. In general,
420 our model works well at the site scale, with average CV-R² values of 0.77, 0.72, and 0.72, and
421 NRMSE values of 0.25, 0.43, and 0.26 for surface NO₂, SO₂, and CO, respectively. In addition,
422 approximately 93%, 80%, and 84% of the stations had at least moderate agreements (CV-R² > 0.6)
423 between our estimates and ground measurements. Except for some scattered sites, the estimation
424 uncertainties were generally less than 0.3, 0.5, and 0.3 in more than 80%, 77%, and 76% of the
425 stations for the above three gaseous pollutant species, respectively.

426 *[Please insert Figure 11 here]*

427 Figure 12 shows the temporal validation of ground-level gaseous pollutants as a function of ground
428 measurements in China. On the monthly scale (Figure 12a-c), we collected a total of ~119,000
429 matched samples of the three gaseous pollutants. Accuracies significantly improved, with increasing
430 R² (decreasing RMSE) values of 0.93 (4.41 µg/m³), 0.97 (4.03 µg/m³), and 0.94 (0.13 mg/m³) for

431 surface NO₂, SO₂, and CO, respectively. On the annual scale (Figure 12d-f), more than ~10,000
432 matched samples were collected, showing better agreement with observations (e.g., $R^2 = 0.94, 0.98,$
433 and 0.97) and lower uncertainties (e.g., RMSE = 3.06 $\mu\text{g}/\text{m}^3$, 2.46 $\mu\text{g}/\text{m}^3$, and 0.07 mg/m^3) for the
434 above three gaseous pollutants, respectively.

435 *[Please insert Figure 12 here]*

436 **3.3.2 Comparison with previous studies**

437 We compared our results with those from previous studies on the estimation of the three gaseous
438 pollutants using different developed models focusing on the whole of China. Here, only those
439 studies applying the same out-of-sample cross-validation approach against ground-based
440 measurements collected from the same CNEMC network were selected (Table 2). The statistics
441 shown in the table come from the publications themselves because their generated datasets are not
442 publicly available. We have applied the same validation method and ground measurements as those
443 used in the previous studies. Most generated surface NO₂ datasets had numerous missing values in
444 space limited by direct OMI/Aura satellite observations at spatial resolutions from $0.125^\circ \times 0.125^\circ$
445 to $0.25^\circ \times 0.25^\circ$ (Chen et al., 2019; Chi et al., 2021; Dou et al., 2021; Xu et al., 2019; Zhan et al.,
446 2018). Some studies improved the spatial resolution by introducing NO₂ data from the recently
447 launched Sentinel-5 TROPOMI satellite, but data are only available from October 2018 onward
448 (Chi et al., 2022; Liu, 2021; Wang et al., 2021; Wei et al., 2022b). Surface SO₂ estimated from an
449 SO₂ emission inventory and surface CO from Measurement of Pollution in the Troposphere
450 (MOPITT) and TROPOMI retrievals have a much lower data quality, with smaller R^2 values by 12–
451 57% and larger RMSE values by 41–47% against ground measurements compared to ours (Li et al.,
452 2020; Liu et al., 2019; Wang et al., 2021). Overall, our gaseous pollutant datasets are superior to
453 those from previous studies in terms of overall accuracy, spatial coverage, and length of data
454 records.

455 *[Please insert Table 2 here]*

456 **3.4 Successful applications**

Our surface gaseous pollutant datasets have been freely available to the public online since March 2021 (See data availability). A large number of studies have used the three gaseous pollutant datasets generated in this study to study their single or joint impacts on environmental health from both long-term and short-term perspectives, benefiting from the unique daily spatially seamless coverage. For example, a nearly linear relationship between long-term ambient NO₂ and adult mortality in China was observed (Zhang et al., 2022b); ambient NO₂ hindered the survival of middle-aged and elderly people (Wang et al., 2023) while acute exposure to ambient SO₂ increased the risk of asthma mortality in China (Li et al., 2023b; Liu et al., 2022b; Liu et al., 2023). Long-term SO₂ and CO exposure can increase the incidence rate of visual impairment in children in China (Chen et al., 2022a), and short-term exposure to ambient CO can significantly increase the probability of hospitalization for stroke sequelae (Wang et al., 2022b). Regional and national cohort studies have shown that exposure, especially short-term exposure, to multiple ambient gaseous (NO₂, SO₂, and CO) and particulate pollutants have negative effects of varying degrees on a variety of diseases, like all-cause mortality (Feng et al., 2023), dementia mortality (Liu et al., 2022a), myocardial infarction mortality (Ma et al., 2023), cause-specific cardiovascular disease (Xu et al., 2022a; Xu et al., 2022b), respiratory diseases (Li et al., 2023a), ischemic and hemorrhagic stroke (Cai et al., 2022; He et al., 2022a; Wu et al., 2022b; Xu et al., 2022c), metabolic syndrome (Guo et al., 2022; Han et al., 2022a), influenza-like illness (Lu et al., 2023), incident dyslipidemia (Hu et al., 2023), diabetes (Mei et al., 2023), blood pressure (Song et al., 2022; Wu et al., 2022a), renal/ kidney function (Li et al., 2022c; Li et al., 2023c), neurodevelopmental delay (Su et al., 2022), serum liver enzymes (Li et al., 2022d), overweight and obesity (Chen et al., 2022b), insomnia (Xu et al., 2021), and sleep quality (Wang et al., 2022a). These studies attest well to the value of the CHAP dataset regarding current and future public health issues, among others.

4. Summary and conclusions

Exposure to gaseous pollution is detrimental to human health, a major public concern in heavily polluted regions like China, where ground-based observations are not as rich as in major developed countries. Moreover, pollutants travel long distances, affecting large downstream regions. To remedy such limitations, this study applied the machine-learning model called Space-Time Extra-

486 Tree to estimate ambient gaseous pollutants across China, with extensive input variables measured
 487 by monitors and satellites, and models. Daily 10 km resolution (approximately $0.1^{\circ} \times 0.1^{\circ}$) seamless
 488 (spatial coverage = 100%) datasets for ground-level NO₂, SO₂, and CO concentrations in China
 489 from 2013 to 2020 were generated. These datasets were cross-evaluated in terms of overall
 490 accuracy and predictive ability at different spatiotemporal levels. National daily estimates
 491 (predictions) of surface NO₂, SO₂, and CO were highly consistent with ground measurements, with
 492 average out-of-sample (out-of-station) CV-R² values of 0.84 (0.68), 0.84 (0.7), and 0.8 (0.61), and
 493 RMSEs of 7.99 (11.57) $\mu\text{g}/\text{m}^3$, 10.7 (14.28) $\mu\text{g}/\text{m}^3$, and 0.29 (0.42) mg/m^3 , respectively.
 494 Ambient pollutant gases varied significantly in space and time, with high levels mainly found in the
 495 North China Plain, especially in winter, due to more anthropogenic emissions, such as coal burning
 496 for heating. All gaseous pollutants sharply declined in China during the COVID-19 outbreak, while
 497 large differences were observed during their recovery times. For example, surface CO was the first
 498 to return to its historical level within the fifth week after the Lunar New Year in 2020, about twice
 499 faster as surface NO₂ and SO₂ levels. This is attributed to more home cooking and enhanced
 500 atmospheric oxidation. Temporally, surface NO₂, SO₂, and CO levels in China gradually decreased
 501 from peaks in 2013 (average = $21.3 \pm 8.8 \mu\text{g}/\text{m}^3$, $23.1 \pm 13.3 \mu\text{g}/\text{m}^3$, and $1.01 \pm 0.29 \text{mg}/\text{m}^3$,
 502 respectively), with annual rates of decrease of $0.23 \mu\text{g}/\text{m}^3$, $2.01 \mu\text{g}/\text{m}^3$, and $0.05 \text{mg}/\text{m}^3$,
 503 respectively ($p < 0.001$), until 2020. Improvements in air quality have been made in the last eight
 504 years, thanks to the implementation of a series of environmental protection policies, greatly
 505 reducing pollutant emissions. In addition, both the areal extents of regions experiencing gaseous
 506 pollution and the probability of gaseous pollution occurring have gradually decreased over time,
 507 especially for surface CO and SO₂, which have almost reached the short-term air quality guidelines
 508 level recommended by the WHO in most areas in China in 2020. This high-quality daily seamless
 509 dataset of gaseous pollutants will benefit future environmental and health-related studies focused on
 510 China, especially studies investigating short-term air pollution exposure.
 511 Although a lot of new and/or useful data and analyses are presented in this study, they still suffer
 512 from some limitations. For example, our estimated surface SO₂ and CO concentrations should have
 513 larger uncertainties than those of NO₂ since model simulations instead of satellite retrievals are
 514 supplemented during modelling to compensate for the lack of data in China. However, these data

often have large biases in the remote regions with few observations as in western China (Li et al., 2022b), as the surface measurements from MEE are mainly over eastern China. More influential factors stemming from regional economic and development differences, and more parameters describing the complex meteorological system (e.g., winds at 850 hPa and the pressure system in the mid-troposphere) need to be considered in developing more powerful artificial intelligence models, which could be helpful in improving the accuracy of air pollutant retrievals. The spatiotemporal resolutions of gaseous pollutants will be further improved by integrating information from polar-orbiting and geostationary satellites to investigate diurnal variations. In a future study, we will also reconstruct data records over the last two decades and investigate their long-term spatiotemporal variations, filling the gap of missing observations. This will help us understand their formation mechanisms and impacts on fine particulate matter and ozone pollution in China.

Data availability

CNEMC measurements of gaseous pollutants are available at <http://www.cnemc.cn>. The reconstructed OMI/Aura tropospheric NO₂ product is available at <https://doi.org/10.6084/m9.figshare.13126847>. MODIS series products and the MERRA-2 reanalysis are available at <https://search.earthdata.nasa.gov/>. The SRTM DEM is available at <https://www2.jpl.nasa.gov/srtm/>, and LandScanTM population information is available at <https://landscan.ornl.gov/>. The ERA5 reanalysis is available at <https://cds.climate.copernicus.eu/>, GEOS CF data are available at <https://portal.nccs.nasa.gov/datashare/gmao/>, and the CAMS reanalysis and emission inventory are available at <https://ads.atmosphere.copernicus.eu/>.

The ChinaHighAirPollutants (CHAP) dataset is open access and freely available at <https://weijing-rs.github.io/product.html>. The ChinaHighNO₂ dataset is available at <https://doi.org/10.5281/zenodo.4641542>, the ChinaHighSO₂ dataset is available at <https://doi.org/10.5281/zenodo.4641538>, and the ChinaHighCO dataset is available at <https://doi.org/10.5281/zenodo.4641530>.

Author contributions

544 JiW and ZL designed the study. JiW performed the research and wrote the initial draft of this paper.
545 ZL, JuW, CL, and PG reviewed and edited the paper. MC copyedited the article. All authors made
546 substantial contributions to this work.

547

548 **Competing interests**

549 The authors declare that they have no conflict of interest.

550

551 **Acknowledgments**

552 JiW, ZL, and JuW were supported by NASA Earth Sciences' Applied Science Programs
553 (80NSSC21K1980 and 80NSSC19K0950). PG was supported by NASA's Research Opportunities
554 in Space and Earth Science (ROSES-2020), Program Element A.38: Health and Air Quality
555 Applied Sciences Team.

References

- Anenberg, S. C., Mohegh, A., Goldberg, D. L., Kerr, G. H., Brauer, M., Burkart, K., Hystad, P., Larkin, A., Wozniak, S., and Lamsal, L.: Long-term trends in urban NO₂ concentrations and associated paediatric asthma incidence: estimates from global datasets, *The Lancet Planetary Health*, 6, e49-e58, [https://doi.org/10.1016/S2542-5196\(21\)00255-2](https://doi.org/10.1016/S2542-5196(21)00255-2), 2022.
- Cai, M., Zhang, S., Lin, X., Qian, Z., McMillin, S. E., Yang, Y., Zhang, Z., Pan, J., and Lin, H.: Association of Ambient Particulate Matter Pollution of Different Sizes With In-Hospital Case Fatality Among Stroke Patients in China, *Neurology*, 10.1212/WNL.0000000000200546, <https://doi.org/10.1212/WNL.0000000000200546>, 2022.
- Chen, L., Wei, J., Ma, T., Gao, D., Wang, X., Wen, B., Chen, M., Li, Y., Jiang, J., Wu, L., Li, W., Liu, X., Song, Y., Guo, X., Dong, Y., and Ma, J.: Ambient gaseous pollutant exposure and incidence of visual impairment among children and adolescents: findings from a longitudinal, two-center cohort study in China, *Environmental Science and Pollution Research*, <https://doi.org/10.1007/s11356-022-20025-3>, 2022a.
- Chen, L., Gao, D., Ma, T., Chen, M., Li, Y., Ma, Y., Wen, B., Jiang, J., Wang, X., Zhang, J., Chen, S., Wu, L., Li, W., Liu, X., Guo, X., Huang, S., Wei, J., Song, Y., Ma, J., and Dong, Y.: Could greenness modify the effects of physical activity and air pollutants on overweight and obesity among children and adolescents?, *Science of The Total Environment*, 832, 155117, <https://doi.org/10.1016/j.scitotenv.2022.155117>, 2022b.
- Chen, Z.-Y., Zhang, R., Zhang, T.-H., Ou, C.-Q., and Guo, Y.: A kriging-calibrated machine learning method for estimating daily ground-level NO₂ in mainland China, *Science of The Total Environment*, 690, 556-564, <https://doi.org/10.1016/j.scitotenv.2019.06.349>, 2019.
- Chi, Y., Fan, M., Zhao, C., Sun, L., Yang, Y., Yang, X., and Tao, J.: Ground-level NO₂ concentration estimation based on OMI tropospheric NO₂ and its spatiotemporal characteristics in typical regions of China, *Atmospheric Research*, 264, 105821, <https://doi.org/10.1016/j.atmosres.2021.105821>, 2021.
- Chi, Y., Fan, M., Zhao, C., Yang, Y., Fan, H., Yang, X., Yang, J., and Tao, J.: Machine learning-based estimation of ground-level NO₂ concentrations over China, *Science of The Total Environment*, 807, 150721, <https://doi.org/10.1016/j.scitotenv.2021.150721>, 2022.
- Cooper, M. J., Martin, R. V., Hammer, M. S., Levelt, P. F., Veefkind, P., Lamsal, L. N., Krotkov, N. A., Brook, J. R., and McLinden, C. A.: Global fine-scale changes in ambient NO₂ during COVID-19 lockdowns, *Nature*, 601, 380-387, 10.1038/s41586-021-04229-0, 2022.
- Dickerson, R. R., Li, C., Li, Z., Marufu, L. T., Stehr, J. W., McClure, B., Krotkov, N., Chen, H., Wang, P., Xia, X., Ban, X., Gong, F., Yuan, J., and Yang, J.: Aircraft observations of dust and pollutants over northeast China: Insight into the meteorological mechanisms of transport, *Journal of Geophysical Research: Atmospheres*, 112, <https://doi.org/10.1029/2007JD008999>, 2007.
- Ding, J., van der A, R. J., Eskes, H. J., Mijling, B., Stavrou, T., van Geffen, J. H. G. M., and Veefkind, J. P.: NO_x Emissions Reduction and Rebound in China Due to the COVID-19 Crisis, *Geophysical Research Letters*, 47, e2020GL089912, <https://doi.org/10.1029/2020GL089912>, 2020.
- Dou, X., Liao, C., Wang, H., Huang, Y., Tu, Y., Huang, X., Peng, Y., Zhu, B., Tan, J., Deng, Z., Wu, N., Sun, T., Ke, P., and Liu, Z.: Estimates of daily ground-level NO₂ concentrations in China based on Random Forest model integrated K-means, *Advances in Applied Energy*, 2, 100017,

<https://doi.org/10.1016/j.adapen.2021.100017>, 2021.

Feng, C., Yu, B., Fei, T., Jia, P., Dou, Q., and Yang, S.: Association between residential greenness and all-cause mortality and the joint mediation effect of air pollutants among old people with disability: A prospective cohort study, *Science of The Total Environment*, 858, 159604, <https://doi.org/10.1016/j.scitotenv.2022.159604>, 2023.

Field, R. D., Hickman, J. E., Geogdzhayev, I. V., Tsigaridis, K., and Bauer, S. E.: Changes in satellite retrievals of atmospheric composition over eastern China during the 2020 COVID-19 lockdowns, *Atmospheric Chemistry and Physics*, 21, 18333-18350, <https://doi.org/10.5194/acp-21-18333-2021>, 2021.

Gao, J., Yang, Y., Wang, H., Wang, P., Li, H., Li, M., Ren, L., Yue, X., and Liao, H.: Fast climate responses to emission reductions in aerosol and ozone precursors in China during 2013–2017, *Atmospheric Chemistry and Physics*, 22, 7131-7142, [10.5194/acp-22-7131-2022](https://doi.org/10.5194/acp-22-7131-2022), 2022.

Geurts, P., Ernst, D., and Wehenkel, L.: Extremely Randomized Trees, *Machine Learning*, 36, 3--42, <https://doi.org/10.1007/s10994-006-6226-1>, 2006.

Guo, Q., Zhao, Y., Zhao, J., Bian, M., Qian, L., Xue, T., Zhang, J., and Duan, X.: Physical activity attenuated the associations between ambient air pollutants and metabolic syndrome (MetS): A nationwide study across 28 provinces, *Environmental Pollution*, 315, 120348, <https://doi.org/10.1016/j.envpol.2022.120348>, 2022.

Han, S., Zhang, F., Yu, H., Wei, J., Xue, L., Duan, Z., and Niu, Z.: Systemic inflammation accelerates the adverse effects of air pollution on metabolic syndrome: Findings from the China health and Retirement Longitudinal Study (CHARLS), *Environmental Research*, 215, 114340, <https://doi.org/10.1016/j.envres.2022.114340>, 2022a.

Han, W., He, T. L., Tang, Z., Wang, M., Jones, D., and Jiang, Z.: A comparative analysis for a deep learning model (hyDL-CO v1.0) and Kalman filter to predict CO concentrations in China, *Geoscientific Model Development*, 15, 4225-4237, <https://doi.org/10.5194/gmd-15-4225-2022>, 2022b.

He, F., Wei, J., Dong, Y., Liu, C., Zhao, K., Peng, W., Lu, Z., Zhang, B., Xue, F., Guo, X., and Jia, X.: Associations of ambient temperature with mortality for ischemic and hemorrhagic stroke and the modification effects of greenness in Shandong Province, China, *Science of The Total Environment*, 158046, <https://doi.org/10.1016/j.scitotenv.2022.158046>, 2022a.

He, J., Gong, S., Yu, Y., Yu, L., Wu, L., Mao, H., Song, C., Zhao, S., Liu, H., Li, X., and Li, R.: Air pollution characteristics and their relation to meteorological conditions during 2014–2015 in major Chinese cities, *Environmental Pollution*, 223, 484-496, <https://doi.org/10.1016/j.envpol.2017.01.050>, 2017.

He, L., Wei, J., Wang, Y., Shang, Q., Liu, J., Yin, Y., Frankenberg, C., Jiang, J. H., Li, Z., and Yung, Y. L.: Marked Impacts of Pollution Mitigation on Crop Yields in China, *Earth's Future*, 10, e2022EF002936, <https://doi.org/10.1029/2022EF002936>, 2022b.

He, Q., Qin, K., Cohen, J. B., Loyola, D., Li, D., Shi, J., and Xue, Y.: Spatially and temporally coherent reconstruction of tropospheric NO₂ over China combining OMI and GOME-2B measurements, *Environmental Research Letters*, 15, 125011, <https://doi.org/10.1088/1748-9326/abc7df>, 2020.

Hersbach, H., Bell, B., Berrisford, P., Hirahara, S., Horányi, A., Muñoz-Sabater, J., Nicolas, J., Peubey, C., Radu, R., Schepers, D., Simmons, A., Soci, C., Abdalla, S., Abellan, X., Balsamo, G., Bechtold, P., Biavati, G., Bidlot, J., Bonavita, M., De Chiara, G., Dahlgren, P., Dee, D.,

644 Diamantakis, M., Dragani, R., Flemming, J., Forbes, R., Fuentes, M., Geer, A., Haimberger, L.,
645 Healy, S., Hogan, R. J., Hólm, E., Janisková, M., Keeley, S., Laloyaux, P., Lopez, P., Lupu, C.,
646 Radnoti, G., de Rosnay, P., Rozum, I., Vamborg, F., Villaume, S., and Thépaut, J.-N.: The
647 ERA5 global reanalysis, *Quarterly Journal of the Royal Meteorological Society*, 146, 1999-
648 2049, <https://doi.org/10.1002/qj.3803>, 2020.

649 Hu, M., Wei, J., Hu, Y., Guo, X., Li, Z., Liu, Y., Li, S., Xue, Y., Li, Y., Liu, M., Wang, L., and Liu,
650 X.: Long-term effect of submicronic particulate matter (PM₁) and intermodal particulate
651 matter (PM_{1-2.5}) on incident dyslipidemia in China: A nationwide 5-year cohort study,
652 *Environmental Research*, 217, 114860, <https://doi.org/10.1016/j.envres.2022.114860>, 2023.

653 Huang, X., Ding, A., Gao, J., Zheng, B., Zhou, D., Qi, X., Tang, R., Wang, J., Ren, C., Nie, W., Chi,
654 X., Xu, Z., Chen, L., Li, Y., Che, F., Pang, N., Wang, H., Tong, D., Qin, W., Cheng, W., Liu, W.,
655 Fu, Q., Liu, B., Chai, F., Davis, S. J., Zhang, Q., and He, K.: Enhanced secondary pollution
656 offset reduction of primary emissions during COVID-19 lockdown in China, *National Science*
657 *Review*, 8, <https://doi.org/10.1093/nsr/nwaa137>, 2020.

658 Inness, A., Ades, M., Agustí-Panareda, A., Barré, J., Benedictow, A., Blechschmidt, A. M.,
659 Dominguez, J. J., Engelen, R., Eskes, H., Flemming, J., Huijnen, V., Jones, L., Kipling, Z.,
660 Massart, S., Parrington, M., Peuch, V. H., Razinger, M., Remy, S., Schulz, M., and Suttie, M.:
661 The CAMS reanalysis of atmospheric composition, *Atmospheric Chemistry and Physics*, 19,
662 3515-3556, <https://doi.org/10.5194/acp-19-3515-2019>, 2019.

663 Jiang, X., Li, G., and Fu, W.: Government environmental governance, structural adjustment and air
664 quality: A quasi-natural experiment based on the Three-year Action Plan to Win the Blue Sky
665 Defense War, *Journal of Environmental Management*, 277, 111470,
666 <https://doi.org/10.1016/j.jenvman.2020.111470>, 2021.

667 Kan, H., Chen, R., and Tong, S.: Ambient air pollution, climate change, and population health in
668 China, *Environment International*, 42, 10-19, <https://doi.org/10.1016/j.envint.2011.03.003>,
669 2012.

670 Koukouli, M. E., Theys, N., Ding, J., Zyrichidou, I., Mijling, B., Balis, D., and van der A, R. J.:
671 Updated SO₂ emission estimates over China using OMI/Aura observations, *Atmospheric*
672 *Measurement Techniques*, 11, 1817-1832, <https://doi.org/10.5194/amt-11-1817-2018>, 2018.

673 Lee, E. J., Kim, M. J., and Lee, J.-S.: Policy Implications of the Clean Heating Transition: A Case
674 Study of Shanxi, *Energies*, 14, 8431, 2021.

675 Levelt, P. F., Stein Zweers, D. C., Aben, I., Bauwens, M., Borsdorff, T., De Smedt, I., Eskes, H. J.,
676 Lerot, C., Loyola, D. G., Romahn, F., Stavrou, T., Theys, N., Van Roozendaal, M., Veefkind,
677 J. P., and Verhoelst, T.: Air quality impacts of COVID-19 lockdown measures detected from
678 space using high spatial resolution observations of multiple trace gases from Sentinel-
679 5P/TROPOMI, *Atmospheric Chemistry and Physics*, 22, 10319-10351,
680 <https://doi.org/10.5194/acp-22-10319-2022>, 2022.

681 Li, C., Hammer, M. S., Zheng, B., and Cohen, R. C.: Accelerated reduction of air pollutants in
682 China, 2017-2020, *Science of The Total Environment*, 803, 150011,
683 <https://doi.org/10.1016/j.scitotenv.2021.150011>, 2022a.

684 Li, H., Yang, Y., Wang, H., Wang, P., Yue, X., and Liao, H.: Projected Aerosol Changes Driven by
685 Emissions and Climate Change Using a Machine Learning Method, *Environmental Science &*
686 *Technology*, 56, 3884-3893, [10.1021/acs.est.1c04380](https://doi.org/10.1021/acs.est.1c04380), 2022b.

687 Li, H., Liang, L., Zhang, S., Qian, Z., Cai, M., Wang, X., McMillin, S. E., Keith, A. E., Wei, J.,

688 Geng, Y., and Lin, H.: Short-term ambient particulate matter pollution of different sizes and
689 respiratory hospital admission in the Beibu Gulf area of Southern China, *Atmospheric*
690 *Environment*, 294, 119524, <https://doi.org/10.1016/j.atmosenv.2022.119524>, 2023a.

691 Li, R., Cui, L., Liang, J., Zhao, Y., Zhang, Z., and Fu, H.: Estimating historical SO₂ level across the
692 whole China during 1973–2014 using random forest model, *Chemosphere*, 247, 125839,
693 <https://doi.org/10.1016/j.chemosphere.2020.125839>, 2020.

694 Li, R., Wang, Z., Cui, L., Fu, H., Zhang, L., Kong, L., Chen, W., and Chen, J.: Air pollution
695 characteristics in China during 2015–2016: Spatiotemporal variations and key meteorological
696 factors, *Science of The Total Environment*, 648, 902–915,
697 <https://doi.org/10.1016/j.scitotenv.2018.08.181>, 2019.

698 Li, S., Wei, J., Hu, Y., Liu, Y., Hu, M., Shi, Y., Xue, Y., Liu, M., Xie, W., Guo, X., and Liu, X.:
699 Long-term effect of intermediate particulate matter (PM_{1–2.5}) on incident asthma among
700 middle-aged and elderly adults: A national population-based longitudinal study, *Science of The*
701 *Total Environment*, 859, 160204, <https://doi.org/10.1016/j.scitotenv.2022.160204>, 2023b.

702 Li, S., Meng, Q., Laba, C., Guan, H., Wang, Z., Pan, Y., Wei, J., Xu, H., Zeng, C., Wang, X., Jiang,
703 M., Lu, R., Guo, B., and Zhao, X.: Associations between long-term exposure to ambient air
704 pollution and renal function in Southwest China: The China Multi-Ethnic Cohort (CMEC)
705 study, *Ecotoxicology and Environmental Safety*, 242, 113851,
706 <https://doi.org/10.1016/j.ecoenv.2022.113851>, 2022c.

707 Li, T., Shen, H., Yuan, Q., Zhang, X., and Zhang, L.: Estimating Ground-Level PM_{2.5} by Fusing
708 Satellite and Station Observations: A Geo-Intelligent Deep Learning Approach, 44, 11,985-
709 911,993, <https://doi.org/10.1002/2017GL075710>, 2017b.

710 Li, Y., Yuan, X., Wei, J., Sun, Y., Ni, W., Zhang, H., Zhang, Y., Wang, R., Xu, R., Chen, G., Liu, Y.,
711 and Xu, J.: Long-term exposure to ambient particulate matter and kidney function in older
712 adults, *Atmospheric Environment*, 295, 119535,
713 <https://doi.org/10.1016/j.atmosenv.2022.119535>, 2023c.

714 Li, Y., Yuan, X., Wei, J., Sun, Y., Ni, W., Zhang, H., Zhang, Y., Wang, R., Xu, R., Liu, T., Yang, C.,
715 Chen, G., Xu, J., and Liu, Y.: Long-term exposure to ambient air pollution and serum liver
716 enzymes in older adults: A population-based longitudinal study, *Annals of Epidemiology*, 74,
717 1–7, <https://doi.org/10.1016/j.annepidem.2022.05.011>, 2022d.

718 Li, Z., Guo, J., Ding, A., Liao, H., Liu, J., Sun, Y., Wang, T., Xue, H., Zhang, H., and Zhu, B.:
719 Aerosol and boundary-layer interactions and impact on air quality, *National Science Review*, 4,
720 810–833, <https://doi.org/10.1093/nsr/nwx117>, 2017a.

721 Lin, J., Lin, C., Tao, M., Ma, J., Fan, L., Xu, R.-A., and Fang, C.: Spatial Disparity of
722 Meteorological Impacts on Carbon Monoxide Pollution in China during the COVID-19
723 Lockdown Period, *ACS Earth and Space Chemistry*, 5, 2900–2909,
724 <https://doi.org/10.1021/acsearthspacechem.1c00251>, 2021.

725 Ling, C. and Li, Y.: Substantial Changes of Gaseous Pollutants and Health Effects During the
726 COVID-19 Lockdown Period Across China, *GeoHealth*, 5, e2021GH000408,
727 <https://doi.org/10.1029/2021GH000408>, 2021.

728 Liu, D., Di, B., Luo, Y., Deng, X., Zhang, H., Yang, F., Grieneisen, M. L., and Zhan, Y.: Estimating
729 ground-level CO concentrations across China based on the national monitoring network and
730 MOPITT: potentially overlooked CO hotspots in the Tibetan Plateau, *Atmospheric Chemistry*
731 *and Physics*, 19, 12413–12430, <https://doi.org/10.5194/acp-19-12413-2019>, 2019.

732 Liu, J.: Mapping high resolution national daily NO₂ exposure across mainland China using an
733 ensemble algorithm, *Environmental Pollution*, 279, 116932,
734 <https://doi.org/10.1016/j.envpol.2021.116932>, 2021.

735 Liu, T., Zhou, Y., Wei, J., Chen, Q., Xu, R., Pan, J., Lu, W., Wang, Y., Fan, Z., Li, Y., Xu, L., Cui, X.,
736 Shi, C., Zhang, L., Chen, X., Bao, W., Sun, H., and Liu, Y.: Association between short-term
737 exposure to ambient air pollution and dementia mortality in Chinese adults, *Science of The*
738 *Total Environment*, 849, 157860, <https://doi.org/10.1016/j.scitotenv.2022.157860>, 2022a.

739 Liu, W., Cai, M., Long, Z., Tong, X., Li, Y., Wang, L., Zhou, M., Wei, J., Lin, H., and Yin, P.:
740 Association between ambient sulfur dioxide pollution and asthma mortality: Evidence from a
741 nationwide analysis in China, *Ecotoxicology and Environmental Safety*, 249, 114442,
742 <https://doi.org/10.1016/j.ecoenv.2022.114442>, 2023.

743 Liu, W., Wei, J., Cai, M., Qian, Z., Long, Z., Wang, L., Vaughn, M. G., Aaron, H. E., Tong, X., Li,
744 Y., Yin, P., Lin, H., and Zhou, M.: Particulate matter pollution and asthma mortality in China:
745 A nationwide time-stratified case-crossover study from 2015 to 2020, *Chemosphere*, 308,
746 136316, <https://doi.org/10.1016/j.chemosphere.2022.136316>, 2022b.

747 Lu, J., Wu, K., Ma, X., Wei, J., Yuan, Z., Huang, Z., Fan, W., Zhong, Q., Huang, Y., and Wu, X.:
748 Short-term effects of ambient particulate matter (PM₁, PM_{2.5} and PM₁₀) on influenza-like
749 illness in Guangzhou, China, *International Journal of Hygiene and Environmental Health*, 247,
750 114074, <https://doi.org/10.1016/j.ijheh.2022.114074>, 2023.

751 Ma, X., Duan, H., Zhang, H., Liu, X., Sun, X., Wei, J., Zhao, M., and Xi, B.: Short-term effects of
752 PM₁, PM_{2.5}, and PM_{2.5} constituents on myocardial infarction mortality in qingdao, China: A
753 time-stratified case-crossover analysis, *Atmospheric Environment*, 294, 119478,
754 <https://doi.org/10.1016/j.atmosenv.2022.119478>, 2023.

755 Ma, Z., Dey, S., Christopher, S., Liu, R., Bi, J., Balyan, P., and Liu, Y.: A review of statistical
756 methods used for developing large-scale and long-term PM_{2.5} models from satellite data,
757 *Remote Sensing of Environment*, 269, 112827, <https://doi.org/10.1016/j.rse.2021.112827>, 2022.

758 Maji, K. J. and Sarkar, C.: Spatio-temporal variations and trends of major air pollutants in China
759 during 2015–2018, *Environmental Science and Pollution Research*, 27, 33792-33808,
760 <https://doi.org/10.1007/s11356-020-09646-8>, 2020.

761 MEE: Technical regulation for selection of ambient air quality monitoring stations (on trial) (in
762 Chinese), Ministry of Ecology and Environment of the People's Republic of China, available
763 at:
764 <https://www.mee.gov.cn/ywgz/fgbz/bz/bzwb/jcffbz/201309/W020131105548727856307.pdf>,
765 2013a.

766 MEE: Specifications and Test Procedures for Ambient Air Quality Continuous Automated
767 Monitoring System for SO₂, NO₂, O₃ and CO (HJ 654-2013) (in Chinese), Ministry of
768 Ecology and Environment of the People's Republic of China, available at:
769 https://www.mee.gov.cn/ywgz/fgbz/bz/bzwb/jcffbz/201308/t20130802_20256853.shtml,
770 2013b.

771 MEE: Technical Specifications for Installation and Acceptance of Ambient Air Quality Continuous
772 Automated Monitoring System for SO₂, NO₂, O₃ and CO (HJ 193-2013) (in Chinese),
773 Ministry of Ecology and Environment of the People's Republic of China, 2013c.

774 MEE: Revision of the Ambien air quality standards (GB 3095-2012) (in Chinese), Ministry of
775 Ecology and Environment of the People's Republic of China, available at:

776 http://www.mee.gov.cn/xxgk2018/xxgk/xxgk2001/201808/t20180815_20629602.html, 2018a.

777 MEE: Technical specifications for operation and quality control of ambient air quality continuous

778 automated monitoring system for SO₂, NO₂, O₃ and CO (HJ 818-2018) (in Chinese), Ministry

779 of Ecology and Environment of the People's Republic of China, available at:

780 http://www.cnemc.cn/jcgf/dqhj/202009/t20200922_20799646.shtml, 2018b.

781 Mei, Y., Li, A., Zhao, J., Zhou, Q., Zhao, M., Xu, J., Li, R., Li, Y., Li, K., Ge, X., Guo, C., Wei, Y.,

782 and Xu, Q.: Association of long-term air pollution exposure with the risk of prediabetes and

783 diabetes: Systematic perspective from inflammatory mechanisms, glucose homeostasis

784 pathway to preventive strategies, *Environmental Research*, 216, 114472,

785 <https://doi.org/10.1016/j.envres.2022.114472>, 2023.

786 Muñoz-Sabater, J., Dutra, E., Agustí-Panareda, A., Albergel, C., Arduini, G., Balsamo, G., Boussetta,

787 S., Choulga, M., Harrigan, S., Hersbach, H., Martens, B., Miralles, D. G., Piles, M.,

788 Rodríguez-Fernández, N. J., Zsoter, E., Buontempo, C., and Thépaut, J. N.: ERA5-Land: a

789 state-of-the-art global reanalysis dataset for land applications, *Earth System Science Data*, 13,

790 4349-4383, <https://doi.org/10.5194/essd-13-4349-2021>, 2021.

791 Murray, C. J. L., Aravkin, A. Y., Zheng, P., and al., e.: Global burden of 87 risk factors in 204

792 countries and territories, 1990–2019: a systematic analysis for the Global Burden of

793 Disease Study 2019, *The Lancet*, 396, 1223-1249, [https://doi.org/10.1016/S0140-](https://doi.org/10.1016/S0140-6736(20)30752-2)

794 [6736\(20\)30752-2](https://doi.org/10.1016/S0140-6736(20)30752-2), 2020.

795 Orellano, P., Reynoso, J., Quaranta, N., Bardach, A., and Ciapponi, A.: Short-term exposure to

796 particulate matter (PM₁₀ and PM_{2.5}), nitrogen dioxide (NO₂), and ozone (O₃) and all-cause

797 and cause-specific mortality: Systematic review and meta-analysis, *Environment International*,

798 142, 105876, <https://doi.org/10.1016/j.envint.2020.105876>, 2020.

799 Qin, K., Rao, L., Xu, J., Bai, Y., Zou, J., Hao, N., Li, S., and Yu, C.: Estimating Ground Level NO₂

800 Concentrations over Central-Eastern China Using a Satellite-Based Geographically and

801 Temporally Weighted Regression Model, *Remote Sensing*, 9, 950, 2017.

802 Rodriguez, J. D., Perez, A., and Lozano, J. A.: Sensitivity Analysis of k-Fold Cross Validation in

803 Prediction Error Estimation, *IEEE Transactions on Pattern Analysis and Machine Intelligence*,

804 32, 569-575, <https://doi.org/10.1109/TPAMI.2009.187>, 2010.

805 Seo, J., Kim, J. Y., Youn, D., Lee, J. Y., Kim, H., Lim, Y. B., Kim, Y., and Jin, H. C.: On the

806 multiday haze in the Asian continental outflow: the important role of synoptic conditions

807 combined with regional and local sources, *Atmospheric Chemistry and Physics*, 17, 9311-9332,

808 <https://doi.org/10.5194/acp-17-9311-2017>, 2017.

809 Shah, V., Jacob, D. J., Li, K., Silvern, R. F., Zhai, S., Liu, M., Lin, J., and Zhang, Q.: Effect of

810 changing NO_x lifetime on the seasonality and long-term trends of satellite-observed

811 tropospheric NO₂ columns over China, *Atmospheric Chemistry and Physics*, 20, 1483-1495,

812 <https://doi.org/10.5194/acp-20-1483-2020>, 2020.

813 Song, J., Du, P., Yi, W., Wei, J., Fang, J., Pan, R., Zhao, F., Zhang, Y., Xu, Z., Sun, Q., Liu, Y., Chen,

814 C., Cheng, J., Lu, Y., Li, T., Su, H., and Shi, X.: Using an Exposome-Wide Approach to

815 Explore the Impact of Urban Environments on Blood Pressure among Adults in Beijing–

816 Tianjin–Hebei and Surrounding Areas of China, *Environmental Science & Technology*,

817 <https://doi.org/10.1021/acs.est.1c08327>, 2022.

818 Su, T., Li, Z., Zheng, Y., Luan, Q., and Guo, J.: Abnormally Shallow Boundary Layer Associated

819 With Severe Air Pollution During the COVID-19 Lockdown in China, *Geophysical Research*

Letters, 47, e2020GL090041, <https://doi.org/10.1029/2020GL090041>, 2020.

Su, X., Zhang, S., Lin, Q., Wu, Y., Yang, Y., Yu, H., Huang, S., Luo, W., Wang, X., Lin, H., Ma, L., and Zhang, Z.: Prenatal exposure to air pollution and neurodevelopmental delay in children: A birth cohort study in Foshan, China, *Science of The Total Environment*, 816, 151658, <https://doi.org/10.1016/j.scitotenv.2021.151658>, 2022.

Tian, H., Liu, Y., Li, Y., Wu, C.-H., Chen, B., Kraemer, M. U. G., Li, B., Cai, J., Xu, B., Yang, Q., Wang, B., Yang, P., Cui, Y., Song, Y., Zheng, P., Wang, Q., Bjornstad, O. N., Yang, R., Grenfell, B. T., Pybus, O. G., and Dye, C.: An investigation of transmission control measures during the first 50 days of the COVID-19 epidemic in China, *Science*, 368, 638-642, <https://doi.org/10.1126/science.abb6105>, 2020.

van der A, R. J., Mijling, B., Ding, J., Koukouli, M. E., Liu, F., Li, Q., Mao, H., and Theys, N.: Cleaning up the air: effectiveness of air quality policy for SO₂ and NO_x emissions in China, *Atmospheric Chemistry and Physics*, 17, 1775-1789, <https://doi.org/10.5194/acp-17-1775-2017>, 2017.

Wan, J., Qin, C., Wang, Q., Xiao, Y., Niu, R., Li, X., and Su, J.: A Brief Overview of the 13th Five-Year Plan for the Protection of Ecological Environment, in: *Environmental Strategy and Planning in China*, edited by: Wang, J., Wang, X., and Wan, J., Springer Singapore, Singapore, 57-85, https://doi.org/10.1007/978-981-16-6909-5_3, 2022.

Wang, L., Zhang, J., Wei, J., Zong, J., Lu, C., Du, Y., and Wang, Q.: Association of ambient air pollution exposure and its variability with subjective sleep quality in China: A multilevel modeling analysis, *Environmental Pollution*, 312, 120020, <https://doi.org/10.1016/j.envpol.2022.120020>, 2022a.

Wang, R., Xu, R., Wei, J., Liu, T., Ye, Y., Li, Y., Lin, Q., Zhou, Y., Huang, S., Lv, Z., Tian, Q., and Liu, Y.: Short-Term Exposure to Ambient Air Pollution and Hospital Admissions for Sequelae of Stroke in Chinese Older Adults, *GeoHealth*, 6, e2022GH000700, <https://doi.org/10.1029/2022GH000700>, 2022b.

Wang, S., Su, H., Chen, C., Tao, W., Streets, D. G., Lu, Z., Zheng, B., Carmichael, G. R., Lelieveld, J., Pöschl, U., and Cheng, Y.: Natural gas shortages during the "coal-to-gas" transition in China have caused a large redistribution of air pollution in winter 2017, *Proceedings of the National Academy of Sciences*, 117, 31018-31025, <https://doi.org/10.1073/pnas.2007513117>, 2020a.

Wang, Y., Yuan, Q., Li, T., Zhu, L., and Zhang, L.: Estimating daily full-coverage near surface O₃, CO, and NO₂ concentrations at a high spatial resolution over China based on S5P-TROPOMI and GEOS-FP, *ISPRS Journal of Photogrammetry and Remote Sensing*, 175, 311-325, <https://doi.org/10.1016/j.isprsjprs.2021.03.018>, 2021.

Wang, Y., Ma, Y. F., Eskes, H., Inness, A., Flemming, J., and Brasseur, G. P.: Evaluation of the CAMS global atmospheric trace gas reanalysis 2003–2016 using aircraft campaign observations, *Atmospheric Chemistry and Physics*, 20, 4493-4521, <https://doi.org/10.5194/acp-20-4493-2020>, 2020b.

Wang, Y., Luo, S., Wei, J., Yang, Z., Hu, K., Yao, Y., and Zhang, Y.: Ambient NO₂ exposure hinders long-term survival of Chinese middle-aged and older adults, *Science of The Total Environment*, 855, 158784, <https://doi.org/10.1016/j.scitotenv.2022.158784>, 2023.

Wei, J., Li, Z., Guo, J., Sun, L., Huang, W., Xue, W., Fan, T., and Cribb, M.: Satellite-Derived 1-km-Resolution PM₁ Concentrations from 2014 to 2018 across China, *Environmental Science & Technology*, 53, 13265-13274, <https://doi.org/10.1021/acs.est.9b03258>, 2019.

Wei, J., Li, Z., Lyapustin, A., Sun, L., Peng, Y., Xue, W., Su, T., and Cribb, M.: Reconstructing 1-km-resolution high-quality PM_{2.5} data records from 2000 to 2018 in China: spatiotemporal variations and policy implications, *Remote Sensing of Environment*, 252, 112136, <https://doi.org/10.1016/j.rse.2020.112136>, 2021a.

Wei, J., Li, Z., Xue, W., Sun, L., Fan, T., Liu, L., Su, T., and Cribb, M.: The ChinaHighPM10 dataset: generation, validation, and spatiotemporal variations from 2015 to 2019 across China, *Environment International*, 146, 106290, <https://doi.org/10.1016/j.envint.2020.106290>, 2021b.

Wei, J., Li, Z., Li, K., Dickerson, R. R., Pinker, R. T., Wang, J., Liu, X., Sun, L., Xue, W., and Cribb, M.: Full-coverage mapping and spatiotemporal variations of ground-level ozone (O₃) pollution from 2013 to 2020 across China, *Remote Sensing of Environment*, 270, 112775, <https://doi.org/10.1016/j.rse.2021.112775>, 2022a.

Wei, J., Li, Z., Cribb, M., Huang, W., Xue, W., Sun, L., Guo, J., Peng, Y., Li, J., Lyapustin, A., Liu, L., Wu, H., and Song, Y.: Improved 1 km resolution PM_{2.5} estimates across China using enhanced space–time extremely randomized trees, *Atmospheric Chemistry and Physics*, 20, 3273–3289, <https://doi.org/10.5194/acp-20-3273-2020>, 2020.

Wei, J., Liu, S., Li, Z., Liu, C., Qin, K., Liu, X., Pinker, R. T., Dickerson, R. R., Lin, J., Boersma, K. F., Sun, L., Li, R., Xue, W., Cui, Y., Zhang, C., and Wang, J.: Ground-Level NO₂ Surveillance from Space Across China for High Resolution Using Interpretable Spatiotemporally Weighted Artificial Intelligence, *Environmental Science & Technology*, <https://doi.org/10.1021/acs.est.2c03834>, 2022b.

WHO: Coronavirus Disease (COVID-19) Pandemic, The World Health Organization, Available online: <https://www.who.int/emergencies/diseases/novel-coronavirus-2019>, 2020.

WHO: WHO global air quality guidelines. Particulate matter (PM_{2.5} and PM₁₀), ozone, nitrogen dioxide, sulfur dioxide and carbon monoxide, Geneva: World Health Organization, Licence: CC BY-NC-SA 3.0 IGO, Licence: CC BY-NC-SA 3.0 IGO, 2021.

Wu, H., Zhang, Y., Zhao, M., Liu, W., Magnussen, C. G., Wei, J., and Xi, B.: Short-term effects of exposure to ambient PM₁ on blood pressure in children and adolescents aged 9 to 18 years in Shandong Province, China, *Atmospheric Environment*, 283, 119180, <https://doi.org/10.1016/j.atmosenv.2022.119180>, 2022a.

Wu, H., Lu, Z., Wei, J., Zhang, B., Liu, X., Zhao, M., Liu, W., Guo, X., and Xi, B.: Effects of the COVID-19 Lockdown on Air Pollutant Levels and Associated Reductions in Ischemic Stroke Incidence in Shandong Province, China, *Frontiers in Public Health*, 10, <https://doi.org/10.3389/fpubh.2022.876615>, 2022b.

Wu, S., Huang, B., Wang, J., He, L., Wang, Z., Yan, Z., Lao, X., Zhang, F., Liu, R., and Du, Z.: Spatiotemporal mapping and assessment of daily ground NO₂ concentrations in China using high-resolution TROPOMI retrievals, *Environmental Pollution*, 273, 116456, <https://doi.org/10.1016/j.envpol.2021.116456>, 2021.

Wu, X., Yang, Y., Gong, Y., Deng, Z., Wang, Y., Wu, W., Zheng, C., and Zhang, Y.: Advances in air pollution control for key industries in China during the 13th five-year plan, *Journal of Environmental Sciences*, <https://doi.org/10.1016/j.jes.2022.09.008>, 2022c.

Xu, H., Bechle, M. J., Wang, M., Szpiro, A. A., Vedal, S., Bai, Y., and Marshall, J. D.: National PM_{2.5} and NO₂ exposure models for China based on land use regression, satellite measurements, and universal kriging, *Science of The Total Environment*, 655, 423–433, <https://doi.org/10.1016/j.scitotenv.2018.11.125>, 2019.

908 Xu, J., Zhou, J., Luo, P., Mao, D., Xu, W., Nima, Q., Cui, C., Yang, S., Ao, L., Wu, J., Wei, J., Chen,
 909 G., Li, S., Guo, Y., Zhang, J., Liu, Z., and Zhao, X.: Associations of long-term exposure to
 910 ambient air pollution and physical activity with insomnia in Chinese adults, *Science of The*
 911 *Total Environment*, 792, 148197, <https://doi.org/10.1016/j.scitotenv.2021.148197>, 2021.

912 Xu, R., Wei, J., Liu, T., Li, Y., Yang, C., Shi, C., Chen, G., Zhou, Y., Sun, H., and Liu, Y.:
 913 Association of short-term exposure to ambient PM1 with total and cause-specific
 914 cardiovascular disease mortality, *Environment International*, 169, 107519,
 915 <https://doi.org/10.1016/j.envint.2022.107519>, 2022a.

916 Xu, R., Shi, C., Wei, J., Lu, W., Li, Y., Liu, T., Wang, Y., Zhou, Y., Chen, G., Sun, H., and Liu, Y.:
 917 Cause-specific cardiovascular disease mortality attributable to ambient temperature: A time-
 918 stratified case-crossover study in Jiangsu province, China, *Ecotoxicology and Environmental*
 919 *Safety*, 236, 113498, <https://doi.org/10.1016/j.ecoenv.2022.113498>, 2022b.

920 Xu, R., Wang, Q., Wei, J., Lu, W., Wang, R., Liu, T., Wang, Y., Fan, Z., Li, Y., Xu, L., Shi, C., Li, G.,
 921 Chen, G., Zhang, L., Zhou, Y., Liu, Y., and Sun, H.: Association of short-term exposure to
 922 ambient air pollution with mortality from ischemic and hemorrhagic stroke, *European Journal*
 923 *of Neurology*, 29, 1994-2005, <https://doi.org/10.1111/ene.15343>, 2022c.

924 Xu, W. Y., Zhao, C. S., Ran, L., Deng, Z. Z., Liu, P. F., Ma, N., Lin, W. L., Xu, X. B., Yan, P., He,
 925 X., Yu, J., Liang, W. D., and Chen, L. L.: Characteristics of pollutants and their correlation to
 926 meteorological conditions at a suburban site in the North China Plain, *Atmos. Chem. Phys.*, 11,
 927 4353-4369, <https://doi.org/10.5194/acp-11-4353-2011>, 2011.

928 Yang, Y., Ren, L., Wu, M., Wang, H., Song, F., Leung, L. R., Hao, X., Li, J., Chen, L., Li, H., Zeng,
 929 L., Zhou, Y., Wang, P., Liao, H., Wang, J., and Zhou, Z.-Q.: Abrupt emissions reductions
 930 during COVID-19 contributed to record summer rainfall in China, *Nature Communications*, 13,
 931 959, <https://doi.org/10.1038/s41467-022-28537-9>, 2022.

932 Yoo, J.-M., Lee, Y.-R., Kim, D., Jeong, M.-J., Stockwell, W. R., Kundu, P. K., Oh, S.-M., Shin, D.-
 933 B., and Lee, S.-J.: New indices for wet scavenging of air pollutants (O3, CO, NO2, SO2, and
 934 PM10) by summertime rain, *Atmospheric Environment*, 82, 226-237,
 935 <https://doi.org/10.1016/j.atmosenv.2013.10.022>, 2014.

936 Zhan, Y., Luo, Y., Deng, X., Zhang, K., Zhang, M., Grieneisen, M. L., and Di, B.: Satellite-Based
 937 Estimates of Daily NO2 Exposure in China Using Hybrid Random Forest and Spatiotemporal
 938 Kriging Model, *Environmental Science & Technology*, 52, 4180-4189,
 939 10.1021/acs.est.7b05669, 2018.

940 Zhang, B., Rong, Y., Yong, R., Qin, D., Li, M., Zou, G., and Pan, J.: Deep learning for air pollutant
 941 concentration prediction: A review, *Atmospheric Environment*, 290, 119347,
 942 <https://doi.org/10.1016/j.atmosenv.2022.119347>, 2022a.

943 Zhang, C., Liu, C., Hu, Q., Cai, Z., Su, W., Xia, C., Zhu, Y., Wang, S., and Liu, J.: Satellite UV-Vis
 944 spectroscopy: implications for air quality trends and their driving forces in China during 2005–
 945 2017, *Light: Science & Applications*, 8, 100, <https://doi.org/10.1038/s41377-019-0210-6>,
 946 2019a.

947 Zhang, Q., Zheng, Y., Tong, D., Shao, M., Wang, S., Zhang, Y., Xu, X., Wang, J., He, H., Liu, W.,
 948 Ding, Y., Lei, Y., Li, J., Wang, Z., Zhang, X., Wang, Y., Cheng, J., Liu, Y., Shi, Q., Yan, L.,
 949 Geng, G., Hong, C., Li, M., Liu, F., Zheng, B., Cao, J., Ding, A., Gao, J., Fu, Q., Huo, J., Liu,
 950 B., Liu, Z., Yang, F., He, K., and Hao, J.: Drivers of improved PM2.5 air quality in China from
 951 2013 to 2017, 116, 24463-24469, <https://doi.org/10.1073/pnas.1907956116>, 2019b.

952 Zhang, Y., Li, Z., Wei, J., Zhan, Y., Liu, L., Yang, Z., Zhang, Y., Liu, R., and Ma, Z.: Long-term
 953 exposure to ambient NO₂ and adult mortality: A nationwide cohort study in China, *Journal of*
 954 *Advanced Research*, 41, 13-22, <https://doi.org/10.1016/j.jare.2022.02.007>, 2022b.

955 Zhang, Z., Wang, J., Hart, J. E., Laden, F., Zhao, C., Li, T., Zheng, P., Li, D., Ye, Z., and Chen, K.:
 956 National scale spatiotemporal land-use regression model for PM_{2.5}, PM₁₀ and NO₂
 957 concentration in China, *Atmospheric Environment*, 192, 48-54,
 958 <https://doi.org/10.1016/j.atmosenv.2018.08.046>, 2018.

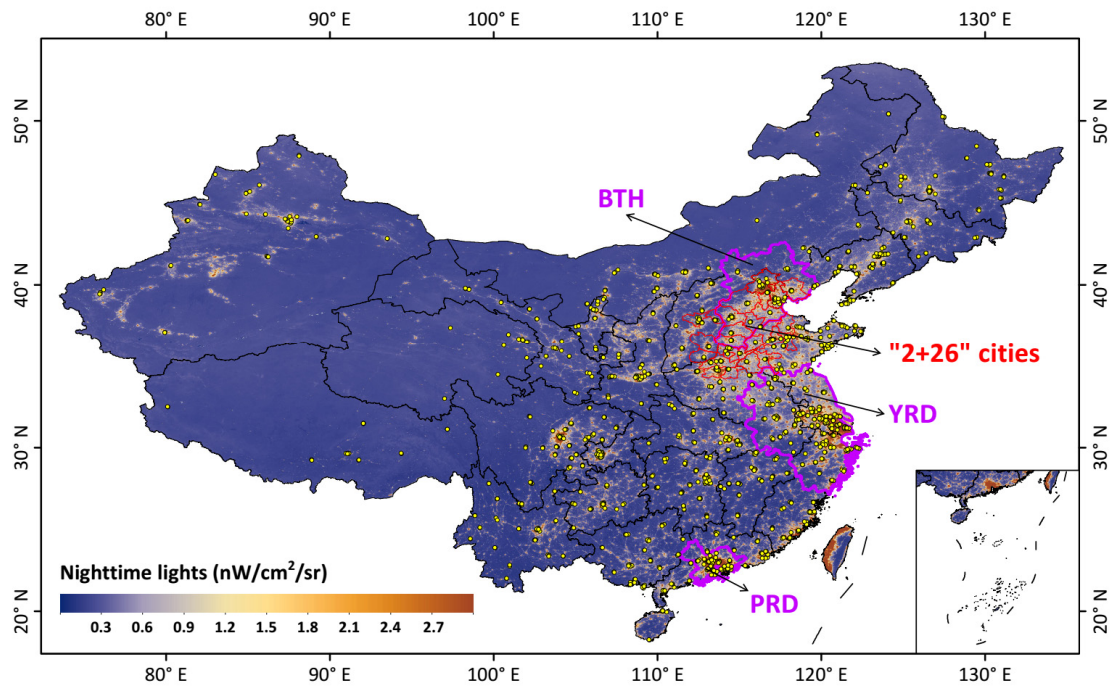
959 Zheng, B., Zhang, Q., Geng, G., Chen, C., Shi, Q., Cui, M., Lei, Y., and He, K.: Changes in China's
 960 anthropogenic emissions and air quality during the COVID-19 pandemic in 2020, *Earth*
 961 *System Science Data*, 13, 2895-2907, <https://doi.org/10.5194/essd-13-2895-2021>, 2021.

962 Zheng, B., Chevallier, F., Ciais, P., Yin, Y., Deeter, M. N., Worden, H. M., Wang, Y., Zhang, Q., and
 963 He, K.: Rapid decline in carbon monoxide emissions and export from East Asia between years
 964 2005 and 2016, *Environmental Research Letters*, 13, 044007, [https://doi.org/10.1088/1748-](https://doi.org/10.1088/1748-9326/aab2b3)
 965 [9326/aab2b3](https://doi.org/10.1088/1748-9326/aab2b3), 2018.

966

967 **Figures**

968



969

970

971

972

973

974

975

Figure 1. Geographical locations of ground-based stations from the China National Environmental Monitoring Centre network (marked as yellow dots) monitoring gaseous pollutants across China. The background shows the nighttime-light level, an estimate of population. Purple boundaries three typical urban agglomerations: the Beijing-Tianjin-Hebei (BTH) region, the Yangtze River Delta (YRD), and the Pearl River Delta (PRD).

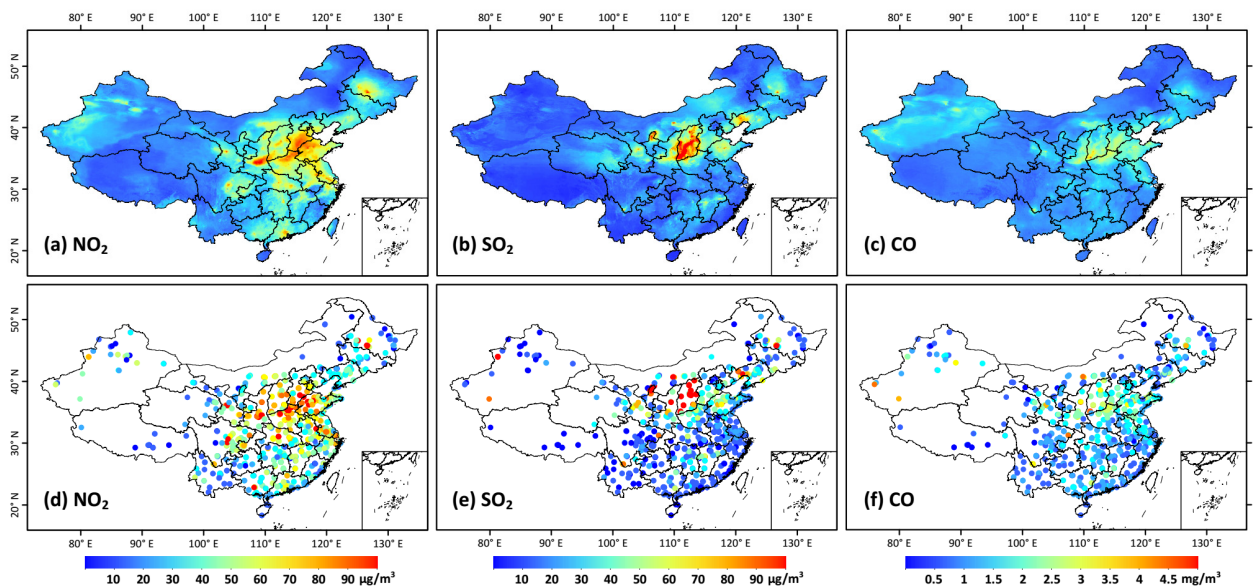


Figure 2. A typical example of (a-c) big-data-derived (horizontal resolution = 10 km) seamless surface NO_2 ($\mu\text{g}/\text{m}^3$), SO_2 ($\mu\text{g}/\text{m}^3$), and CO (mg/m^3) concentrations and (d-f) corresponding ground measurements on 1 January 2018 in China.

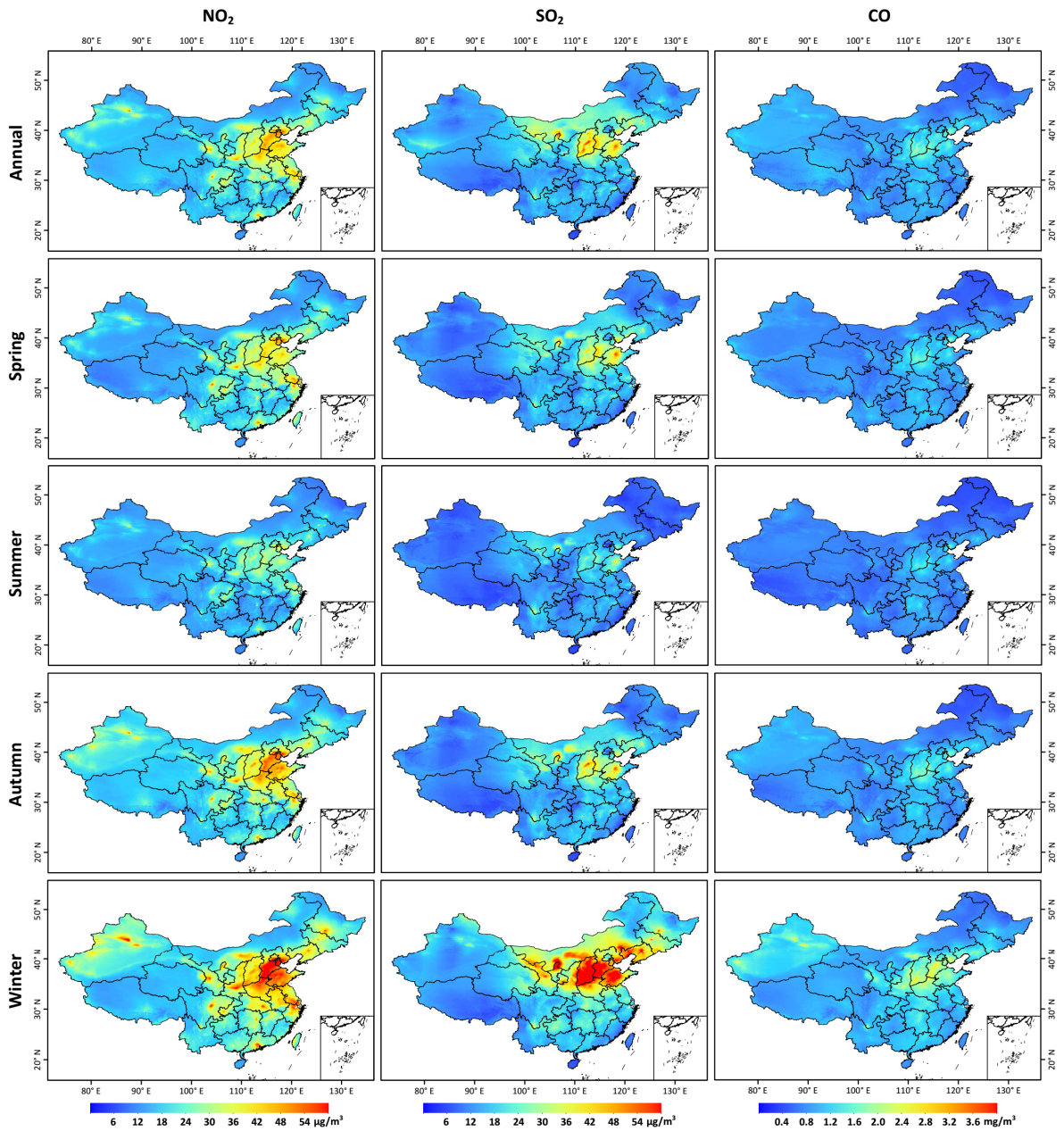


Figure 3. Annual and seasonal mean maps (horizontal resolution = 10 km) of surface NO_2 ($\mu\text{g}/\text{m}^3$), SO_2 ($\mu\text{g}/\text{m}^3$), and CO (mg/m^3) averaged over the period 2013–2020 in China.

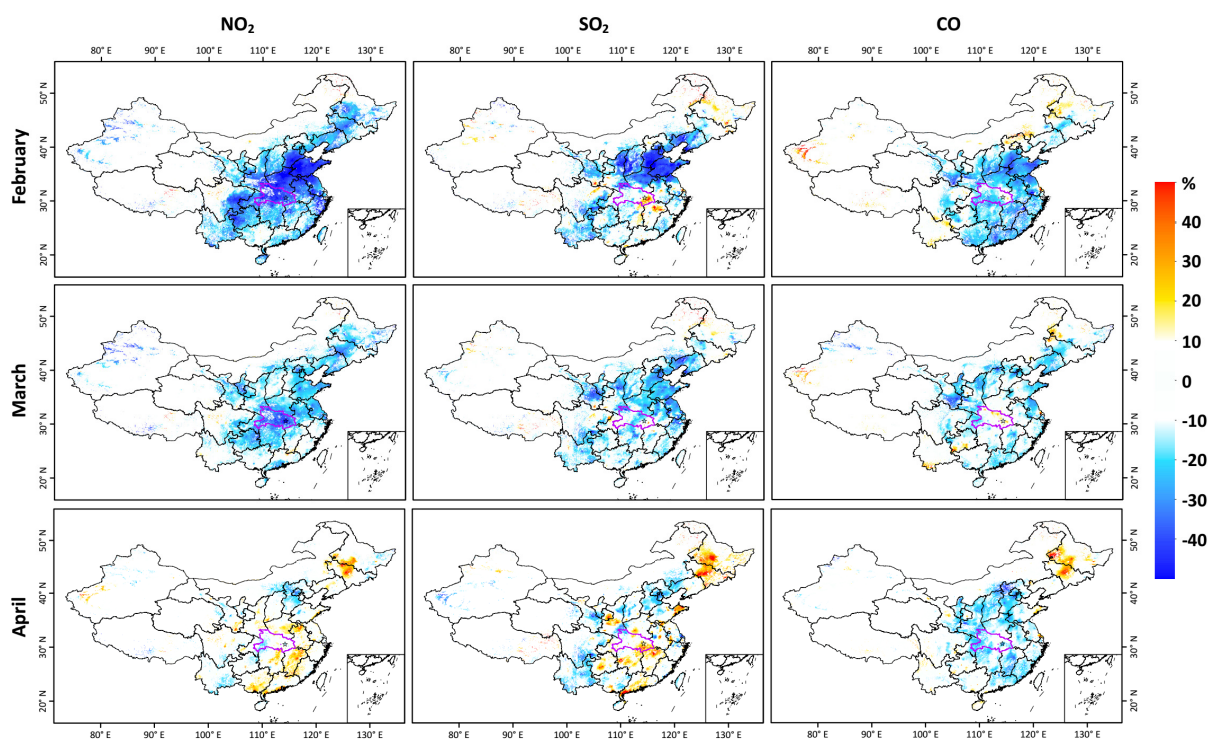


Figure 4. Relative changes (%) in surface NO_2 , SO_2 , and CO concentrations in February, March, and April between 2019 and 2020 in populated areas of China. The area outlined in magenta and the star in each panel indicate Hubei Province and Wuhan City, respectively.

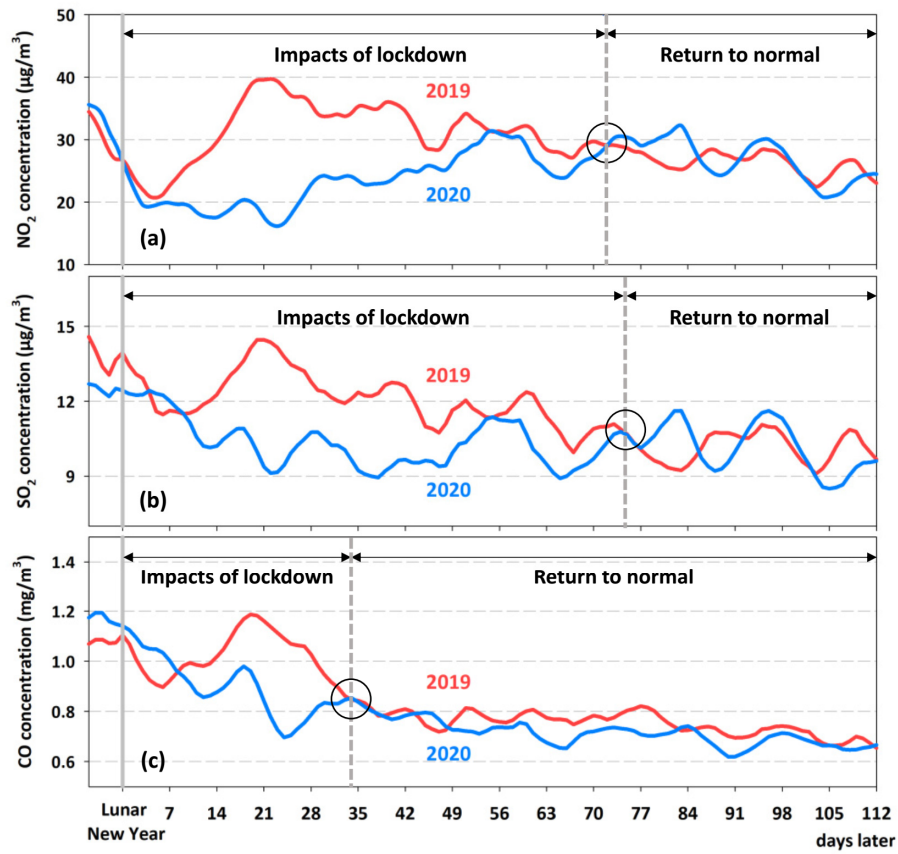


Figure 5. Time series of the seven-day moving averages of daily population-weighted surface (a) NO₂, (b) SO₂, and (c) CO concentrations after the Lunar New Year of 2019 and 2020 in China. The black circle in each panel shows the turning point when the gaseous pollutants began to return to their normal levels.

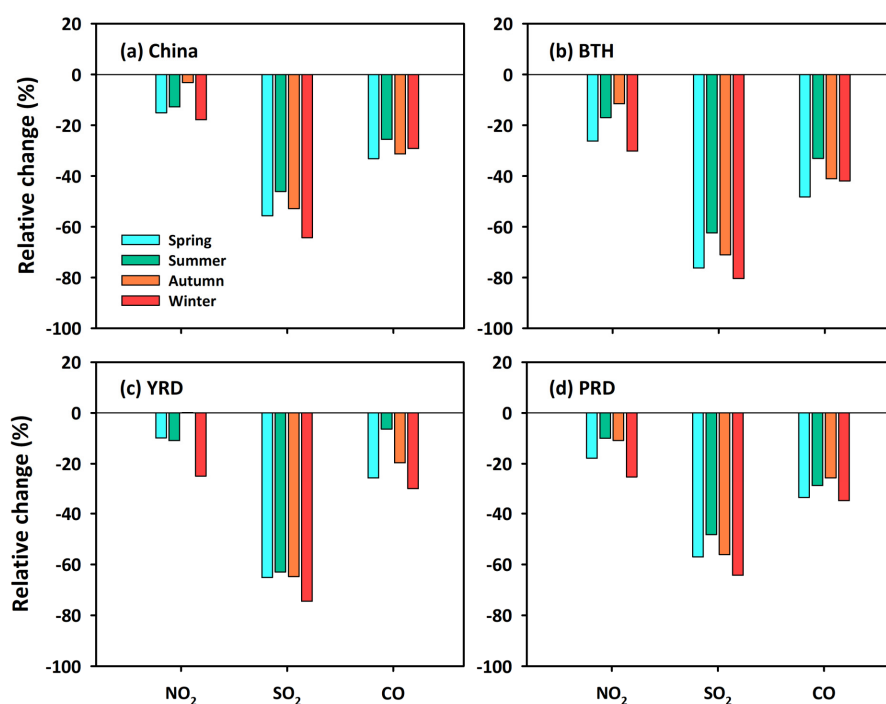


Figure 6. Relative changes (%) in seasonal mean surface NO₂, SO₂, and CO concentrations between 2013 and 2020 over (a) China, (b) the Beijing-Tianjin-Hebei (BTH) region, (c) the Yangtze River Delta (YRD), and (d) the Pearl River Delta (PRD).

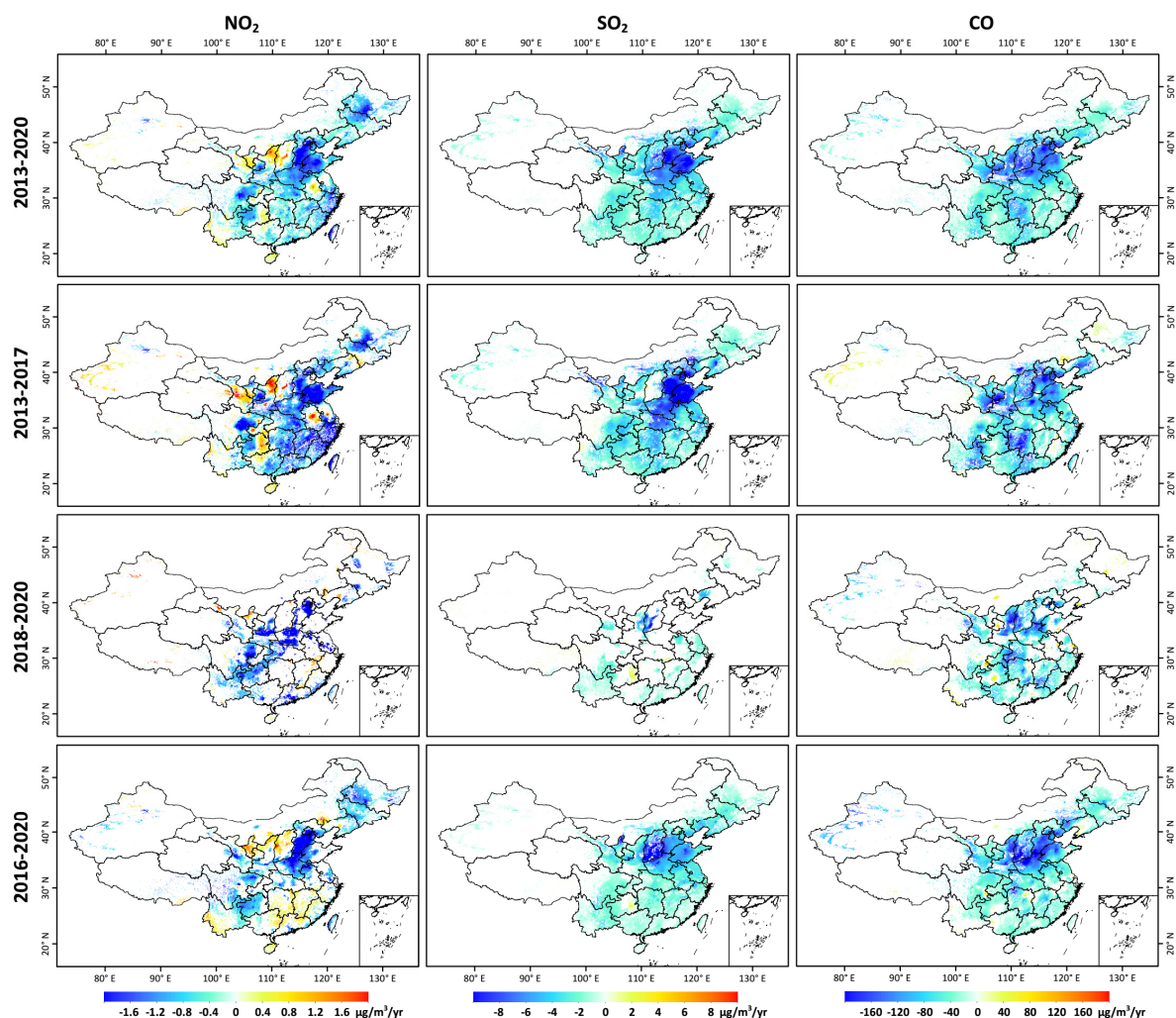


Figure 7. Temporal trends of surface NO_2 , SO_2 , and CO concentrations during the whole period (2013–2020), the Clean Air Action Plan (2013–2017), the Blue Sky Defense War (2018–2020), and the 13rd Five-Year Plan (2016–2020) in populated areas of China. Only regions with trends that are significant at the 95% ($p < 0.05$) confidence level are shown.

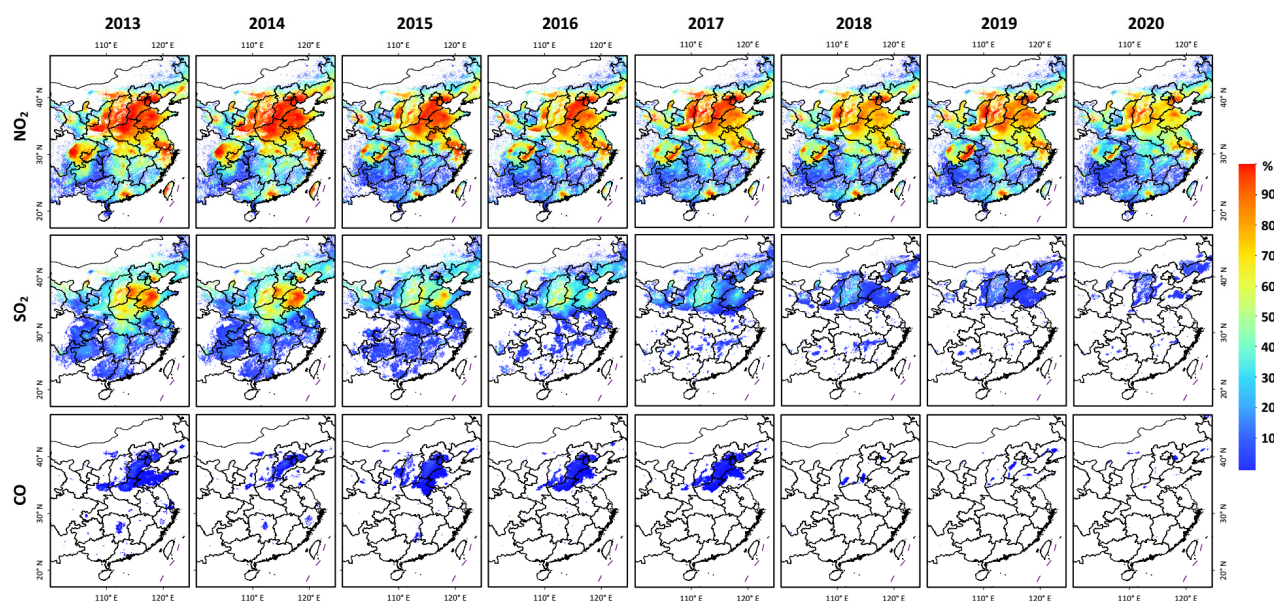


Figure 8. Spatial distributions of the percentage of days exceeding the WHO recommended short-term desired air quality guidelines (AQG) level for surface NO₂ (daily mean > 25 µg/m³), SO₂ (daily mean > 40 µg/m³), and CO (daily mean > 4 mg/m³) for each year from 2013 to 2020 in populated areas of eastern China.

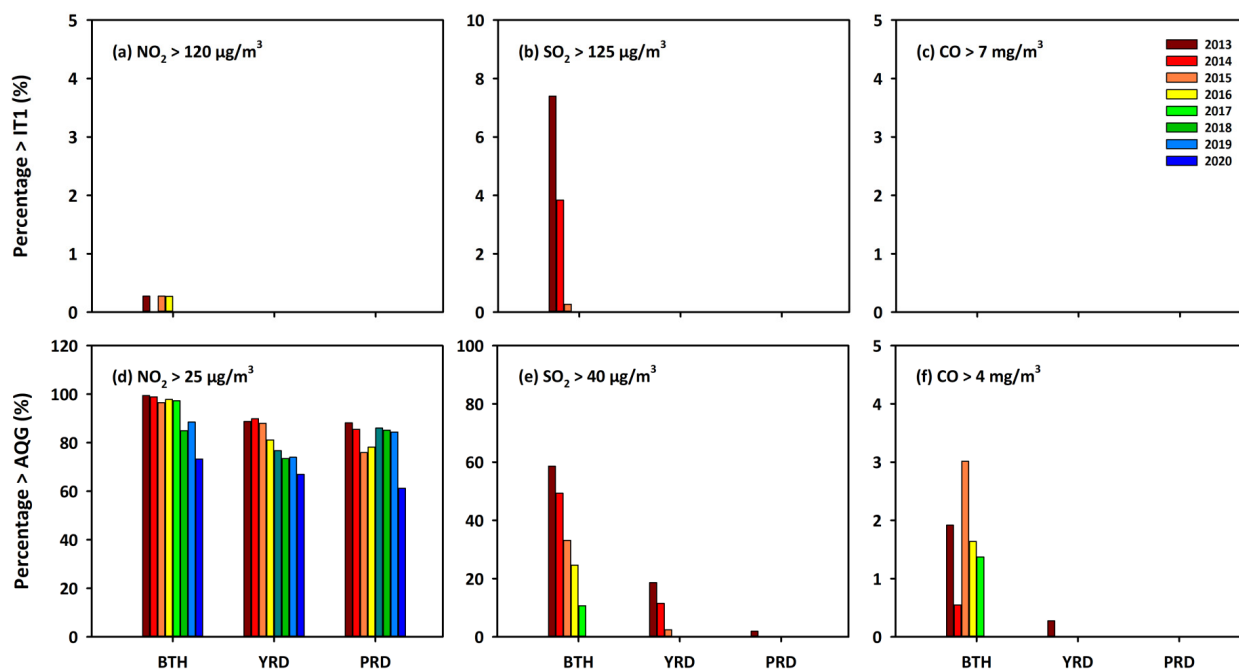


Figure 9. Percentage of days (%) exceeding the WHO recommended short-term (a-c) minimum interim target (IT1) and (d-f) desired air quality guidelines (AQG) level for surface NO₂, SO₂, and CO for each year from 2013 to 2020 in three typical urban agglomerations: the Beijing-Tianjin-Hebei (BTH) region, the Yangtze River Delta (YRD), and the Pearl River Delta (PRD).

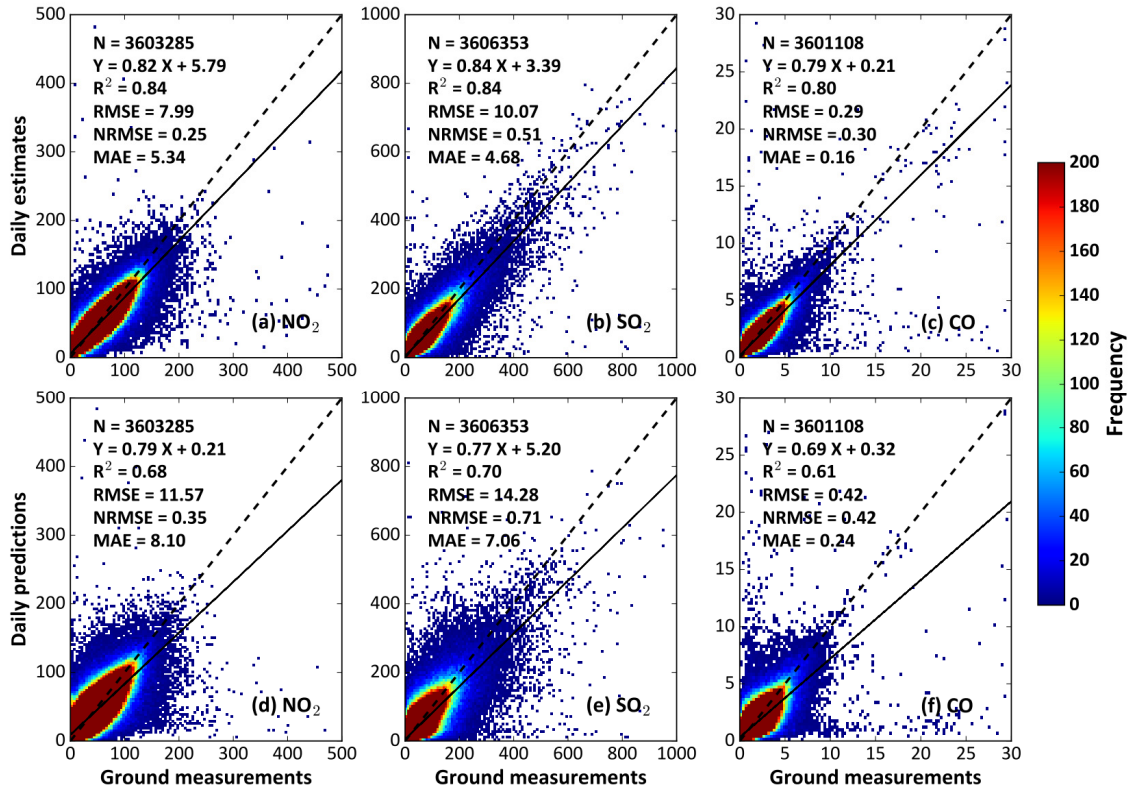


Figure 10. Density plots of daily (a-c) estimates and (d-f) predictions of ground-level NO₂ (µg/m³), SO₂ (µg/m³), and CO (mg/m³) concentrations as a function of ground measurements in China from 2013 to 2020 using the out-of-sample (top panels) and out-of-station (bottom panels) cross-validation methods.

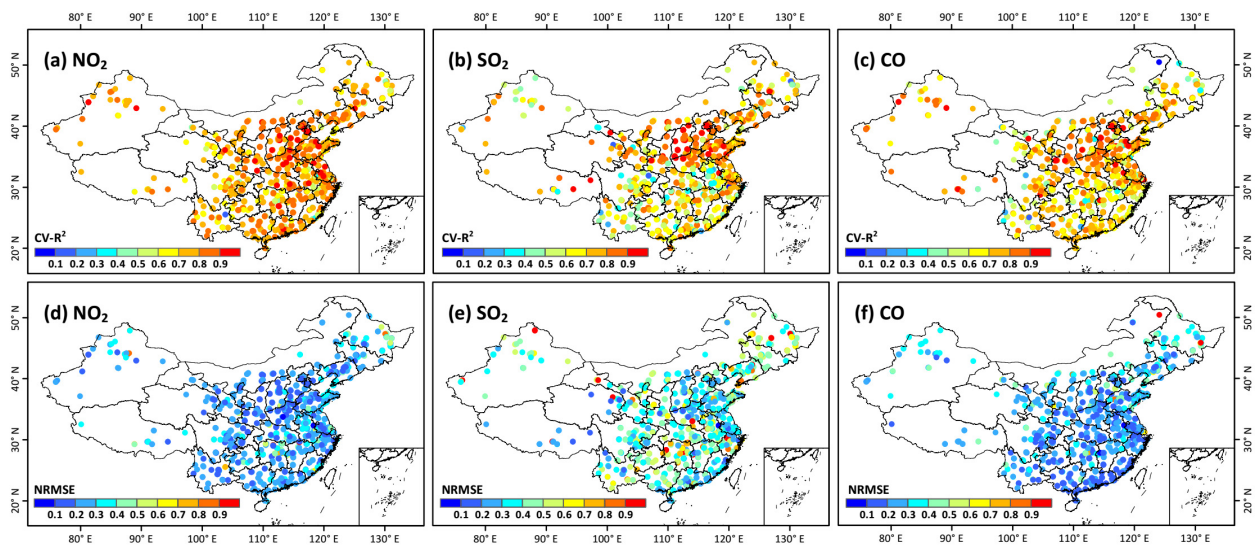


Figure 11. Sample-based spatial validation of daily ground-level NO_2 ($\mu\text{g}/\text{m}^3$), SO_2 ($\mu\text{g}/\text{m}^3$), and CO (mg/m^3) estimates at each individual monitoring station in China from 2013 to 2020: (a-c) accuracy (i.e., CV-R^2) and (d-f) uncertainty (i.e., NRMSE).

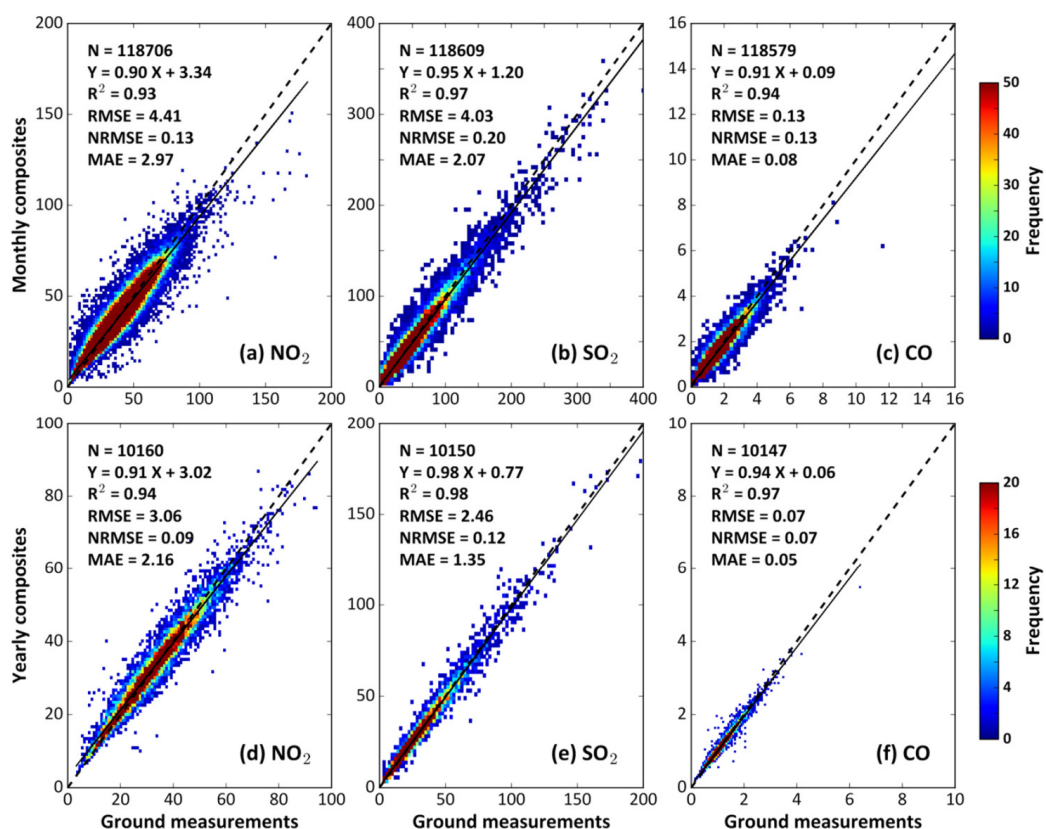


Figure 12. Sample-based temporal validation of (a-c) monthly and (d-f) yearly composites of ground-level NO_2 ($\mu\text{g}/\text{m}^3$), SO_2 ($\mu\text{g}/\text{m}^3$), and CO (mg/m^3) as a function of ground measurements from 2013 to 2020 in China.

1033 **Tables**

1034

1035 **Table 1.** Statistics of the overall accuracies and predictive abilities of ambient gaseous pollutants for

1036 each year in China from 2013 to 2020.

Year	Sample size N (10 ³)	Overall accuracy						Predictive ability					
		NO ₂		SO ₂		CO		NO ₂		SO ₂		CO	
		R ²	RMSE	R ²	RMSE	R ²	RMSE	R ²	RMSE	R ²	RMSE	R ²	RMSE
2013	169	0.77	12.48	0.83	17.97	0.80	0.56	0.53	18.16	0.68	25.04	0.60	0.78
2014	324	0.76	10.97	0.83	15.87	0.77	0.38	0.54	15.56	0.66	22.45	0.51	0.57
2015	518	0.79	9.34	0.80	13.71	0.74	0.38	0.61	13.10	0.61	19.49	0.50	0.55
2016	516	0.82	8.59	0.83	11.26	0.76	0.34	0.64	12.20	0.65	16.28	0.57	0.46
2017	527	0.86	7.57	0.86	7.79	0.82	0.24	0.72	10.67	0.74	10.80	0.70	0.32
2018	513	0.87	6.92	0.83	5.61	0.82	0.20	0.76	9.33	0.68	7.80	0.69	0.26
2019	515	0.87	6.78	0.81	4.84	0.82	0.20	0.77	9.23	0.66	6.63	0.70	0.25
2020	522	0.89	5.78	0.80	4.02	0.82	0.17	0.79	8.04	0.62	5.57	0.69	0.23

1037

1038

Table 2. Comparison of long-term datasets of different gaseous pollutants in China.

Species	Model	Missing values	Spatial resolution	Main input	Validation period	CV-R ²	RMSE	Literature
NO ₂	RF-STK	Yes	0.25°	OMI	2013–2016	0.62	13.3	(Zhan et al., 2018)
	RF-K	Yes	0.25°	OMI	2013–2018	0.64	11.4	(Dou et al., 2021)
	KCS	Yes	0.125°	OMI	2014–2016	0.72	7.9	(Chen et al., 2019)
	LUR	Yes	0.125°	OMI	2014–2015	0.78	-	(Xu et al., 2019)
	LME	Yes	0.1°	OMI	2014–2020	0.65	7.9	(Chi et al., 2021)
	XGBoost	Yes	0.125°	TROPOMI	2018–2020	0.67	6.4	(Chi et al., 2022)
	XGBoost	Yes	0.05°	TROPOMI	2018–2019	0.83	7.6	(Liu, 2021)
	LightGBM	No	0.05°	TROPOMI	2018–2020	0.83	6.6	(Wang et al., 2021)
	SWDF	No	0.01°	TROPOMI	2019–2020	0.93	4.9	(Wei et al., 2022b)
	STET	No	0.1°	Big data	2013–2020	0.84	8.0	This study
SO ₂	RF	No	0.25°	Emissions	2013–2014	0.64	17.1	(Li et al., 2020)
	STET	No	0.1	Big data	2013–2020	0.84	10.1	This study
CO	RF-STK	Yes	0.1	MOPITT	2013–2016	0.51	0.54	(Liu et al., 2019)
	LightGBM	No	0.07°	TROPOMI	2018–2020	0.71	0.26	(Wang et al., 2021)
	STET	No	0.1°	Big data	2013–2020	0.80	0.29	This study

1039

1040

1041

1042

1043

KCS: kriging-calibrated satellite method; LightGBM: light gradient boosted model; LME: linear mixed effect model; LUR: land use regression; MOPITT: Measurements of Pollution in the Troposphere; OMI: Ozone Monitoring Instrument; RF: random forest; RF-K: random forest integrated with K-means; RF-STK: random-forest-spatiotemporal-kriging model; STET: space-time extremely randomized tree; SWDF: spatiotemporally weighted deep forest; TROPOMI: TROPospheric Monitoring Instrument; XGBoost: extreme gradient boosting